Research Square

Preprints are preliminary reports that have not undergone peer review. They should not be considered conclusive, used to inform clinical practice, or referenced by the media as validated information.

# Alkali Activation of Fly Ash in the Presence of Sodium Nitrate

**Ela Ofer-Rozovsky** ( elaof@ariel.ac.il )
Ariel University https://orcid.org/0000-0002-6965-0170

**Gabriela Bar-Nes**
Nuclear Research Centre Negev

**Amnon Katz**
Technion Israel Institute of Technology Faculty of Civil and Environmental Engineering

**Michal Arbel Haddad**
Nuclear Research Centre Negev

**Research Article**

**Keywords:** geopolymers, fly ash, nitrate, zeolites, nitrate-cancrinite.

**Posted Date:** May 28th, 2021

**DOI:** https://doi.org/10.21203/rs.3.rs-521400/v1

**License:** This work is licensed under a Creative Commons Attribution 4.0 International License.
Read Full License

**Version of Record:** A version of this preprint was published at Waste and Biomass Valorization on October 31st, 2021. See the published version at https://doi.org/10.1007/s12649-021-01584-x.

# Abstract

The use of fly ash as a precursor for geopolymer has been investigated during the last decades for various applications. The aim of this research was to study the effect of nitrate on the formation and evolution of fly ash-based geopolymers, in order to assess their applicability as waste immobilization matrices. These may be of interest in order to treat waste streams from agricultural runoff and various industries including the nuclear industry.

Fly ash was alkali-activated using NaOH solutions of various alkalinities, to which nitrates were added as $NaNO_3$. The samples were cured at 40℃ for different periods and characterized by X-Ray diffractometry, Fourier transform mid-Infrared spectroscopy, scanning electron microscopy (SEM), and compressive strength measurements.

The content of neo-formed crystalline phases in fly ash-based geopolymers was found to be lower than in metakaolin-based systems studied previously. The nature of the minerals formed in nitrate-free samples differed from those obtained in corresponding metakaolin-based geopolymers. Nevertheless, the dominant phase formed in the presence of nitrate at sufficiently high alkalinity was nitrate-cancrinite, as reported for metakaolin-based geopolymers, regardless of the type of fly-ash used. Although the presence of nitrates was found to have a promoting effect on the geopolymerization process of metakaolin-based geopolymers, it was found to inhibit the processes in fly-ash-based geopolymers.

The formation of crystalline phases in FA-based geopolymers suggests that these materials may be used for immobilizing various hazardous species, while FA-based geopolymers containing the nitrate-cancrinite can be considered as a promising candidate for immobilizing radionuclides from radioactive wastes.


# Statement Of Novelty

The economic and environmental benefits of using waste materials like fly ash for geopolymer production as an immobilization matrix of toxic and nuclear waste played an important role in the advancement of geopolymer research. Nevertheless, the geopolymerization process and phase evolution within geopolymer matrices prepared using fly-ash as the sole silica and alumina source and activated with waste solution simulants containing nitrates were not examined comprehensively. Nitrates are often present in nuclear waste streams, in agricultural runoff waters, and in industrial waste streams. Therefore, the aim of the present study was to investigate the effect of the nitrate ion on the formation and evolution of fly ash-based geopolymer-zeolite composites, in order to assess their applicability as waste immobilization matrices.

# Introduction

Geopolymers are inorganic polymers prepared by alkaline activation of various alumino-silicate sources. The alumino-silicates are initially hydrolyzed by the alkaline solution, and the resulting monomeric and

oligomeric species eventually polymerize, yielding a 3-D network of tetrahedrally bonded silicate and aluminate groups [1, 2]. While the chemical nature of geopolymers is similar to that of zeolites, their overall porous semi-crystalline structure resembles that of classic cementitious materials. Various alumino-silicate sources, including industrial by-products such as fly ash (FA) and slags, may be used as raw materials for the preparation of geopolymers. The economic and environmental benefits of using waste materials as the alumino-silicate source for geopolymer production played an important role in the advancement of geopolymer research, which had traditionally focused on applications in the construction industry [3]. Nevertheless, various other applications have also been proposed over the years, including the potential use of geopolymer matrices for the immobilization of toxic and nuclear waste [3–5].

The potential use of FA-based geopolymers as immobilization matrices for heavy metals and radionuclides was previously studied by several research groups [6–11]. The negatively-charged alumina groups within the alumino-silicate backbone of the geopolymer serve as cation binding sites, facilitating their immobilization. More recent studies have shown that the formation of crystalline zeolite domains within the amorphous geopolymer matrix further enhances the immobilization of metal cations [9, 11–13]. Furthermore, the geopolymeric monolith serves as a strong and durable mechanical support for the desired zeolites, which also facilitates their handling and serves as an additional barrier between the toxic waste and the environment [10, 14].

Among the many factors influencing the structural evolution of these geopolymer-zeolite composites are the nature of the alumino-silicate precursor, the alkalinity of the activation solution, transient $SiO_2$:$Al_2O_3$ ratios in the geopolymeric gel, the nature of the metal cation present and its content (expressed as $M_2O$:$Al_2O_3$ ratio, M = metal cation), and curing temperature. The extent of zeolite formation within geopolymer matrices is known to depend upon the $SiO_2$:$Al_2O_3$ ratio within the geopolymer mix. High $SiO_2$:$Al_2O_3$ ratios generally lead to the formation of highly amorphous materials, whereas lower ratios are more likely to result in the formation of crystalline zeolite domains embedded within the continuous amorphous geopolymer phase [15, 16]. The formation of crystalline domains may also be enhanced by higher metal cation content ($M_2O$:$Al_2O_3$ ratio [17]) and elevated curing temperatures [18], as well as by post-curing heat treatment [19, 20].

The presence of different anionic species in the activating solution may also affect the rate of geopolymerization processes within the geopolymer gel, thus affecting the structure and properties of the resulting geopolymeric product. The introduction of nitrate or sulfate anions into the activating solution was shown to alter the setting times of high-silica ($SiO_2$:$Al_2O_3$ ratio $\geq 3.6$) MK-based geopolymers [18]. Different trends were observed for Na-based and K-based geopolymers. We have previously reported accelerated formation of the nitrate bearing crystalline phases nitrate-sodalite and nitrate cancrinite in low-silica ($SiO_2$:$Al_2O_3 \approx 2.0$) MK-based geopolymers containing sodium nitrate [17]. Observations regarding the impact of different anions on the mechanical properties of geopolymers also indicate different trends for the different anions studied. In the abovementioned studies, the compressive strength

of geopolymers was found to increase with increasing nitrate content [17, 18]. An increase in compressive strength was also reported in the presence of carbonates in fly ash-kaolin based systems, while chlorides were reported to have a negative impact on the compressive strength of the same systems [21]. A decrease in compressive strength due to the presence of nitrate and sulfate anions was reported in slag-based systems [22, 23].

The study presented here was aimed at investigating the effect of the nitrate ion on the evolution of structure and properties of FA-based geopolymer-zeolite composites, in order to assess their applicability as waste immobilization matrices. Nitrates are often present in nuclear waste streams, in agricultural runoff waters, and in industrial waste streams from fertilizer and metal finishing industries, and are considered an environmental hazard [24]. The geopolymerization process and phase evolution within geopolymer matrices prepared using FA as the sole silica and alumina source activated with waste solution simulants, were followed over three months. The results were compared to those obtained in our previous study using metakaolin (MK), which is often used as a model alumino-silicate precursor due to its low impurity content and high amorphous content which contributes to its reactivity [17].

# Materials And Methods

Three different samples of fly-ash (FA) conforming to EN 450-1 specification for fly ash for concrete were supplied by the “Orot Rabin” station, Israel Electric Company (IEC). The chemical composition of the different ashes (Table 1) was determined using lithium metaborate fusion and ICP (Ion Coupled Plasma) analysis. The physical properties are presented in Table 2. The density was measured using the Le Chatelier method (EN 196-6), the particle distribution by volume was determined by dispersion in water using Mastersizer 2000 (Malvern), and the pozzolanity (activity index) was measured using EN 450-1.

Table 1
Chemical composition of raw fly ashes

| | Oxides, weight (%) | | | | | | | | | | LOI[a] |
|---|---|---|---|---|---|---|---|---|---|---|---|
| | $SiO_2$ | $Al_2O_3$ | $Fe_2O_3$ | CaO | $TiO_2$ | MgO | $Na_2O$ | $K_2O$ | $P_2O_5$ | $SO_3$ | |
| FFA1 | 40.5 | 29.4 | 3.6 | 9.4 | 1.5 | 2.2 | 0.3 | 0.8 | 1.8 | 0.4 | 6.0% |
| FFA2 | 56.3 | 22.1 | 6.0 | 7.7 | 1.0 | 1.6 | 1.5 | 1.3 | 0.2 | 0.8 | 1.2% |
| FFA3 | 59.9 | 22.4 | 6.4 | 3.1 | 1.1 | 1.3 | 0.6 | 1.3 | 0.6 | 0.5 | 2.4% |

[a] LOI: loss on ignition, 950$^{o}$C, EN 450-1

Table 2
Physical characterization of raw fly ashes

| | BET [$m^2/g$] | Density [$g/cm^3$] | Particle size distribution ]μm[ | | | Pozzolanity | | |
|---|---|---|---|---|---|---|---|---|
| | | | D10 | D50 | D90 | 7 days | 28 days | 90 days |
| FA1 | 15.0 | 2.14 | 2.94 | 16.12 | 69.18 | 70% | 79% | 82% |
| FA2 | n/a | 2.21 | 2.13 | 17.99 | 75.72 | 72% | 92% | 98% |
| FA3 | n/a | 2.23 | 4.39 | 25.21 | 106.15 | 64% | 73% | 82% |

# 2.1 Preparation of geopolymers

Geopolymers were prepared from fly ashes described above using either nitrate-free or nitrate-bearing activation solutions similar to those used in our previous studies [12, 13, 17]. The activation solution compositions and mix formulations are presented in Table 3.

Nitrate-free formulations were prepared using NaOH solutions of varying alkalinity, which are denoted by their $H_2O:OH^-$ molar ratios (dilution factor = *d*) of 5.50, 9.15, 13.75, and 27.50, corresponding to approximately 9M, 5.5M, 4M, and 2M NaOH, respectively. The solid:solution ratios of samples prepared from FA1 were adjusted to obtain $Na_2O:Al_2O_3$ ratio of 0.84, 1.00, and 1.20. $Na_2O:Al_2O_3$ ratio of 1.00 was kept when preparing samples from FA2 and FA3, which were examined only at $d = 5.50$.

Sodium nitrate was added to the previously described activating solutions to obtain nitrate-bearing samples. The nitrate content of each of these solutions was denoted by the $NO_3:OH^-$ ($NaNO_3$:NaOH) molar ratio. Three nitrate-bearing activating solutions were prepared from the most alkaline solution NaOH solutions ($d = 5.50$) with $NO_3^-:OH^-$ molar ratios of 0.10, 0.25, and 0.30, thus yielding $Na_2O:Al_2O_3$ ratios of 1.10, 1.25, and 1.30 respectively. Activating solutions of lower alkalinity were prepared with $NO_3^-:OH^-$ ratios of 0.25 and 0.40 ($Na_2O:Al_2O_3$ ratio of 1.25 and 1.40 respectively) in the case of $d = 9.15$, and with $NO_3^-$:OH molar ratio of 0.25 ($Na_2O:Al_2O_3$ ratio of 1.25) for $d = 13.75$ and $d = 27.50$. Here again, the dilution factor used for the nitrate-bearing geopolymer formulations was kept at the same value as their respective reference formulations, resulting in higher $Na_2O:Al_2O_3$ ratios, as specified in Table 3.

FA was mixed manually with the activation solution at ambient temperature for 15 minutes. The samples were cast into polypropylene containers (50 ml test-tubes, 26.5 mm diameter), properly sealed and cured at 40℃ ± 3 for periods ranging from 1 day to 3 months.

Table 3
Activation solution compositions and mix formulations in terms of molar ratios

| Sample name | Activation solutions | | Mix formulations | | |
|---|---|---|---|---|---|
| | $H_2O : OH^-$, d | $NO_3 : OH^-$ | $Na_2O : Al_2O_3$ | $NO_3 : Al_2O_3$ | $H_2O$:FA [g/g] |
| FA1-5.50d-0N | 5.50 | 0 | 1.00 | 0 | 0.57 |
| | | | 1.20 | | 0.67 |
| | | | 0.84 | | 0.48 |
| FA2-5.50d-0N | | | 1.00 | | 0.43 |
| FA3-5.50d-0N | | | 1.00 | | 0.43 |
| FA1-9.15d-0N | 9.15 | | 1.00 | | 0.95 |
| FA1-13.75d-0N | 13.75 | | 1.00 | | 1.42 |
| | | | 1.20 | | 1.70 |
| | | | 0.84 | | 1.19 |
| FA1-27.50d-0N | 27.50 | | 1.00 | | 2.85 |
| FA1-5.50d-1.0N | 5.50 | 0.10 | 1.10 | 0.17 | 0.57 |
| FA1-5.50d-2.5N | | 0.25 | 1.25 | 0.50 | 0.57 |
| | | | 1.50 | 0.60 | 0.67 |
| | | | 1.04 | 0.42 | 0.48 |
| FA1-5.50d-3.0N | | 0.30 | 1.30 | 0.62 | 0.57 |
| FA2-5.50d-2.5N | | 0.25 | 1.25 | 0.50 | 0.43 |
| FA3-5.50d-2.5N | | | 1.25 | | 0.43 |
| FA1-9.15d-1.4N | 9.15 | 0.25 | 1.25 | 0.50 | 0.95 |
| FA1-9.15d-4.0N | | 0.40 | 1.40 | 0.80 | 0.95 |
| FA1-13.75d-1N | 13.75 | 0.25 | 1.25 | 0.50 | 1.42 |
| | | | 1.50 | 0.60 | 1.70 |
| | | | 1.04 | 0.42 | 1.19 |
| FA1-27.50d-0.5N | 27.50 | 0.25 | 1.25 | 0.50 | 2.85 |

## 2.2 Characterization techniques

Samples for XRD (X-Ray diffractometry) and FTIR (Fourier Transform Mid-Infrared spectroscopy) were ground manually using a mortar and pestle. XRD measurements were carried out using the ground samples with no additional treatment. FTIR samples were prepared by pressing a mixture of 2–5 mg ground sample with 100 mg dry KBr into pellets. Samples of the various raw materials were prepared in a similar manner.

The XRD analysis of FA1-based samples was conducted using a SIEMENS D5000 diffractometer using $CuK_{\alpha}$ radiation at 20 kV, 5 mA, and a scanning rate of $0.9^{\circ}$ $min^{-1}$, while PanAnalytical Empyrean Powder diffractometer with $CuK_{\alpha}$ radiation at 40 kV, 30 mA, and a scanning rate of $0.49^{\circ}$/min was used for FA2- and FA3-based samples. In both cases measurements were conducted from $2\theta = 5^{\circ}$ to $2\theta = 80^{\circ}$. Data in the range of $2\theta = 60^{\circ}$-$80^{\circ}$, which did not yield much information, were omitted from the presentation for the sake of clarity. FTIR spectra were collected in the range of 500–1500 $cm^{-1}$ using a BRUKER Vector 22 FTIR spectrometer with 2 $cm^{-1}$ resolution in transmittance mode.

Quantitative XRD analysis using the Rietveld method was performed for nitrate bearing samples ($d$ = 9.15) cured for 1 month, using PowderCell program [25]. Atomic coordinates suggested for amorphous silica [26] were used for simulating the diffraction due to the amorphous phase of the geopolymer. Structural data for zeolites and feldspathoids were taken from Pearson's Crystal Structure Database for Inorganic Compounds [27].

XRD spectra were normalized with respect to the mullite diffraction line at $2\theta = 16.37°$. Mullite is present in FA and remains unaltered throughout the geopolymerization process. Normalization of FTIR spectra was carried out using the integrated intensity in the 900–1300 $cm^{-1}$ range of the spectrum, which is due to the asymmetric stretching vibration of T-O-T (T = Al, Si) bonds. Table 4 summarizes the major absorbance bands due to T-O, T-O-T, and N-O vibrations and their respective identification.

Compressive strength measurements were performed using sets of 3–5 replicate samples. Cylindrical samples with a 26.5 mm diameter and height were obtained by cutting the monoliths extracted from the polypropylene test-tubes to the appropriate height. Samples were polished and then dried for 24 hours in an oven at 40℃ before testing on Amsler press 100 kN.

SEM (scanning electron microscopy) images were obtained using a Jeol 5300 scanning electron microscope (SEM). Fracture surface specimens were observed after drying at 50°C for 24 hours and coating with Au.

Table 4

FTIR absorbance signals of phases observed for raw materials and the FA-based geopolymers [$cm^{-1}$], T = Si, Al

| Phase in geopolymeric matrix | T-O-T stretching mode | | N-O symmetric stretching mode | References |
|---|---|---|---|---|
| | Symmetric (SBUs) | Asymmetric | | |
| **Fly-Ash** | 560 | 1090, 1185 | | [28] |
| **Sodium nitrate** | | | 820, 1383 | [29] |
| **Amorphous geopolymer** | 650–800 | 975–990 | | [30] |
| **Chabazite (CHA)** | 620–660, 715–730 | 975–992 | | [10, 31] |
| **Zeolite P (GIS)** | 660 | 975–995 | | *Current research* |
| **Zeolite X (FAU)** | 695, 746 | 975–990 | | [16, 17] |
| **Nitrate sodalite (SOD)** | 661, 730 | 990 | 1383 | [32, 33] |
| **Nitrate cancrinite (CAN)** | 575, 622, 682 | 961, 999, 1041, 1120 | 1415–1435 | [29] |

# Results

## 3.1 Nitrate-free formulations

### 3.1.1 Activation at high alkalinity: $H_2O$:$OH^-$ molar ratio (*d*) of 5.50

SEM images of the raw FA1 and of the activated FA1 geopolymer (FA1-5.50d-0N, $Na_2O$: $Al_2O_3$ = 1.00) can be seen in **Fig. 1** and **Fig. 2**, respectively. The well-known spherical morphology of fly-ash originating from coal combustion is observed in the raw FA1 (Fig. 1), with sphere diameters ranging from 0.5 µm to 15 µm. After alkaline activation, these intact spheres are no longer observed in **Fig. 2**. Crystalline phases as well as amorphous material are observed in the images 2a, 2c, and 2d. A hollow sphere morphology due to geopolymer setting on the surface of FA spheres is often observed (**Fig. 2d**). The needle-shaped and small-flower-shaped morphologies seen in image **Fig. 2b** are most probably due to zeolitic phases. These observations are due to the formation of the geopolymer matrix, as was reported by others [34–36].

**Figure 3** presents the XRD patterns of samples FA1-5.50d-0N ($Na_2O$: $Al_2O_3$ = 1.00) as a function of curing time. Diffraction lines due to mullite (Powder Diffraction File, PDF #01-089-2645) and quartz (PDF #01-086-1561) which are present in the raw FA1 are also observed in the diffraction patterns of geopolymer

samples. A broad peak centered around 2θ = 31°was initially observed in the diffraction pattern obtained after one day of curing. This peak, which was not observed in the diffraction pattern of FA1, is due to the formation of a geopolymeric gel [16, 17]. This broad peak was also observed in the diffraction patterns of samples after longer curing periods, thus indicating the presence of an amorphous geopolymer phase throughout the time frame studied here.

The appearance of distinct diffraction peaks at 2θ = 13.93°, 24.23°, 34.43° after 3 days of curing is indicative of rearrangement of the amorphous phase into crystalline phases. The observed diffraction peaks may be attributed to a zeolite from a chabazite family with a relatively low $SiO_2$:$Al_2O_3$ ratio of 2, $NaAlSiO_4 \cdot XH_2O$ (PDF #00-044-0248), which was previously reported to form in FA-based geopolymeric systems [37, 38]. Additional peaks belonging to the same crystalline phase at 2θ = 9.33° and 20.63° are observed after a 3 month curing period.

The diffraction patterns of FA1-5.50d-0N samples prepared with different solid:solution ratios, yielding $Na_2O$:$Al_2O_3$ ratios of 1.20 and 0.84, were essentially the same as those obtained for samples with a $Na_2O$:$Al_2O_3$ ratio of 1. This is unlike the result obtained for the corresponding MK-based geopolymers, where the $Na_2O$:$Al_2O_3$ ratio had a significant impact on the relative amount of the two reaction products, which were zeolite A and zeolite X [17].

The effect of fly ash composition is demonstrated in **Fig. 4**, where the diffraction patterns of FA2-5.50d-0N and FA3-5.50d-0N geopolymer samples after 3 months of curing are presented. Diffraction peaks at 2θ = 9.44°, 17.62°, 20.54° are attributed to a chabazite phase with the chemical formula $NaAlSi_2O_6 \cdot 2H_2O$ (PDF #00-019-1178). This phase has a higher Si content than the chabazite phase identified in the diffraction pattern of FA1-5.50d-0N samples (Fig. 3). This is in line with the fact that both FA2 and FA3 have a higher $Si_2O$ content than does FA1 ($SiO_2$:$Al_2O_3$ ratios of 4.3 and 4.6 in FA2 and FA3, respectively, vs 2.3 in FA1) (Table 1).

FTIR spectra of the raw FA1 and of FA1-5.50d-0N ($Na_2O$: $Al_2O_3$ = 1.00) as a function of curing time are presented in **Fig. 5**. The IR absorbance band due to asymmetric stretching of T-O-T (T = Si, Al) in the raw FA is wide, with maximal intensity at 1090 $cm^{-1}$. A shift of the maximal intensity to a lower wavenumber, 1020 $cm^{-1}$, after 1 day of curing, is the first indication of geopolymer formation, in agreement with XRD results. This shift of the asymmetric T-O-T stretching band towards a lower wavenumber is attributed to Al incorporation within the generated alumonosilicate framework of the geopolymer [17, 31]. However, the band at 1098 $cm^{-1}$ indicates that the dissolution of the FA precursor was not complete after one day. An absorption peak at 1262 $cm^{-1}$ is also observed. Absorption at a similar wavenumber was previously reported in FA-based geopolymer gel by Fernandez-Jimenez et al. [31], and is probably due to an intermediate product, as it is no longer observed after 3 days of curing. The main band shifts to 992 $cm^{-1}$ after 3 days of curing and remains at the same wavelength during the next 3 months. It should be noted that the wavenumber of maximal absorption (992 $cm^{-1}$) is higher than in a similar MK-based sample studied (977 $cm^{-1}$) [17] indicating lower Al content in the FA-based geopolymer framework. The

absorbance bands due to stretching modes in mullite at 560 and 1185 $cm^{-1}$ [28] are observed throughout the curing period.

Further indications concerning the rearrangements taking place within the geopolymeric gel could be obtained by following changes in the spectral features which can be attributed to the T-O symmetric stretching and OH bending vibrations of terminal T-OH groups ([16, 17, 39]), which appear in the 830–870 $cm^{-1}$ region of the spectrum. Two distinct vibrations (804, 865 $cm^{-1}$) were observed following 1 day of curing at 40℃, suggesting the existence of at least two different chemical environments near the terminal T-OH groups. The band at 804 $cm^{-1}$ was no longer observed after 3 days of curing, indicating a more homogeneous speciation at this stage of the process. Similar changes in speciation were observed in MK-based geopolymers [17] and are concurrent with the appearance of XRD diffraction peaks due to Na-chabazite (Fig. 3). Absorbance bands in this region (880 – 865 $cm^{-1}$) are also observed for the longer curing times (1 week, 3 months), whereas this band was absent in the corresponding MK-based geopolymers after a 3 months curing period [17]. This indicates that the geopolymerization processes in FA-based systems are slower than in MK-based systems.

The formation of zeolites and related crystalline structures within the geopolymer matrix is usually reflected in the 500–800 $cm^{-1}$ region of the FTIR spectrum, where features due to T-O-T symmetric stretching modes due to specific zeolite secondary building blocks (SBU) may be observed. Figure 5 reveals two absorbance bands this region (around 660, 715 $cm^{-1}$). According to Fernandez et al., absorbance bands in the range of 630–640 $cm^{-1}$ and 720–730 $cm^{-1}$ are characteristic of the D4R and D6R ring vibrations in chabazite zeolites, respectively [31]. It should be noted that the intensity of these bands as well as their resolution are lower than previously observed in parallel MK-based geopolymers, indicating once again that the crystallinity of the FA-based geopolymers is lower. The FTIR spectra also show an absorbance band of the carbonate group at 1420–1490 $cm^{-1}$. Carbonation of the geopolymer sample may have occurred due to exposure to atmospheric conditions during the characterization procedure.

# 3.1.2 Activation at lower alkalinities - d = 9.15, 13.75, 27.50

Activation of FA by solutions of lower alkalinity and consequently higher water content (i.e. *d* values of 9.15, 13.75, and 27.50) is known to delay the geopolymerization process [39]. Much like the products obtained at high alkalinity, XRD data presented in **Fig. 6** indicate that following three months of curing all of the matrices obtained from FA1 at the lower alkalinity values may be described as a composite of an amorphous phase (a broad peak centered around 2θ = 30°) and crystalline phases. However, the crystalline phases formed at lower alkalinities differed from those observed at higher alkalinity. Zeolite X, $Na_2Al_2Si_{2.4}O_{8.8}$•6.7$H_2$0 (main diffraction peak at 2θ = 6.09°, PDF #00-012-0246) belonging to a faujasite group, and zeolite P, $Na_{1.4}Al_2Si_{3.9}O_{11.5}$•$H_2$0 (diffraction peaks at 2θ = 12.77°, 17.90°, 21.98°, 28.13°, 33.50°, PDF #00-046-0103) belonging to a gismondine group are observed in all of the cases studied. Additional

diffraction peaks observed at 2θ = 9.33°, 29.06°, and 29.95° can be attributed to tobermorite, $Ca_5Si_6O_{17}$•$5H_2O$, which is a common phase in products of activation of Ca-rich FA [36, 40].

FTIR spectra for the same samples (Fig. 7) show similar trends as do the XRD patterns. The maximal intensity of the T-O-T asymmetric band observed after 3 months was found to shift from 985 $cm^{-1}$ for samples with the highest alkalinity (*d* = 9.15) to 995 $cm^{-1}$ for the lowest alkalinity (*d* = 27.50). This is indicative of a decrease in Al incorporation into the geopolymeric backbone with decreasing alkalinity. Absorbance bands at ~ 660 $cm^{-1}$ and in the range of 730–746 $cm^{-1}$ are observed in the SBU region of the FTIR spectra. The band at 660 $cm^{-1}$ is due to D4R-ring vibrations (in zeolite X and P), while the absorbance band in the range of 730–746 $cm^{-1}$ is due to D6R-ring vibrations (zeolite X) [31]. The wavenumber of the later absorbance band is found to shift to higher values with the increasing alkalinity, indicating a higher Si content in the D6R rings.

## 3.2 Nitrate-bearing formulations

### 3.2.1 Activation at high alkalinity: $H_2O$:$OH^-$ molar ratio (*d*) of 5.50

The presence of sodium nitrate in the geopolymer mix was found to affect the rate of rearrangements within the geopolymer matrix as well as structure and properties of the resulting geopolymers. Figure 8 shows SEM images of the FA1-5.50d-3.0N sample after 3 months of curing. Two main morphologies can be noticed: the first is of polymerized fly ash spheres and the second of long needles which can be attributed to crystalline phases within the amorphous material. In some locations, the flower-shaped crystals can also be noticed. Despite the similarity with FA1-5.50d-0N samples (Fig. 2), it can be noticed that more FA spheres remained unreacted in presence of nitrate than in the nitrate-free systems.

The diffraction patterns of the geopolymeric matrix FA1-5.50d-2.5N ($Na_2O$: $Al_2O_{3=}$1.00) are presented in **Fig. 9** as a function of curing time. Diffraction peaks due to a crystalline phase within the geopolymer matrix were identified after 3 days of curing. These peaks are associated with nitrate cancrinite, $Na_8Al_6(SiO_4)_6(NO_3)_2{\cdot}4H_2O$, (PDF #00-038-0513), a mineral belonging to the feldspathoid family. The intensity of these peaks increases with curing time, indicating an increase in cancrinite content. The formation of nitrate cancrinite was previously observed in similar MK-based geopolymers, where it was preceded by the formation of nitrate sodalite [17]. These two phases are structurally related, and hence most of the diffraction lines of nitrate-sodalite overlap those of nitrate cancrinite. The presence of nitrate sodalite is usually detected due to relatively weak yet unique diffraction peak at 2θ = 60.03° [17]. The low signal-to-noise ratio in the diffraction pattern presented in Fig. 9 does not allow a clear indication for the presence of this phase within the cured samples, nor does it allow to rule it out.

The FTIR absorbance spectra in **Fig. 10** show that the main absorbance band of the asymmetric stretching vibration of T-O-T bonds (T = Si, Al) shifted from 1090 $cm^{-1}$ in the raw FA1 to 987 $cm^{-1}$ in the geopolymeric matrices after 1 day of curing, indicating that a geopolymeric product had already formed

by this time. No further changes in the position of the T-O-T band were observed within the remaining 3 months of curing. The relative intensity of the terminal T-OH absorbance band in the range of 840–885 $cm^{-1}$ was very high after 1 day of curing but diminished with curing time. However, the persistence of a band in this region after 3 months of curing indicates that rearrangements within the geopolymer matrix still occur throughout this period.

The absorbance bands observed in the 1380–1440 $cm^{-1}$ region may be assigned to the N-O symmetric stretching modes of the nitrate group [33]. The high intensity band at 1383 $cm^{-1}$ is characteristic of nitrate ions in aqueous environments as well as in several crystalline phases (see Table 4) was observed in all of the geopolymer samples studied here. The absorbance bands in the range of 1415–1435 $cm^{-1}$ are characteristic of nitrate ions intercalated within the nitrate cancrinite crystalline phase, which has two different crystallographic positions ([29, 41]). The band at 1415 $cm^{-1}$ can be clearly observed in the FTIR spectrum after 1 day of curing, while the band at 1423 $cm^{-1}$ was observed starting from the next measurement, after 3 days of curing. These 2 bands, together with the bands in the SBU region at 570 $cm^{-1}$, 622 $cm^{-1}$, and 685 $cm^{-1}$, which were previously attributed to nitrate cancrinite [17], support the identification suggested by the XRD data. Here again it should be mentioned that the nitrate cancrinite absorbance bands are not as well resolved as the respective bands observed previously in nitrate-bearing MK-based geopolymers [17]. Moreover, their relative intensity with respect to the strong band at 1383 $cm^{-1}$ is lower than in the MK-based geopolymers, indicating a lower nitrate cancrinite content. These bands are further obscured by the absorbance at 1440 $cm^{-1}$ which is probably due to carbonate, possibly indicating partial carbonation of the cancrinite [42].

**Figure 11** presents the XRD patterns of the FA2-5.50d-2.5N and FA3-5.50d-2.5N geopolymers following 3 months of curing. The main crystalline phase obtained in both cases is nitrate-cancrinite, as in FA1-5.50d-2.5N samples. Diffraction peaks attributed to zeolite X from a faujasite group, a zeolite which was previously reported as an intermediate phase preceding the formation of nitrate-cancrinite ([17, 41]), can also be detected in the XRD pattern of the FA3-based geopolymer. FA3 has a higher $SiO_2$:$Al_2O_3$ ratio, lower LOI, and higher content of Fe than FA1. Furthermore, FA3 has the highest particle size (and consequently the lowest surface area) among the 3 fly ashes. All of these factors may have resulted in a higher content of the intermediate zeolite X phase in FA3-based geopolymers, compared to FA2 and FA1 based geopolymers.

Varying the solid:solution ratios had no effect on the diffraction patterns nor on the FTIR spectra obtained, as found for the nitrate-free formulation and unlike the corresponding MK-based geopolymers, for which the $Na_2O$:$Al_2O_3$ ratio had a significant impact on the reaction rates and products [17].

# 3.2.2 Activation at lower alkalinities - d = 9.15, 13.75, 27.50

**Figure 12** shows the diffraction patterns for geopolymer matrices prepared using the three lower alkalinity activation solutions (*d* = 9.15, 13.75, 27.50) in the presence of nitrate following 3 months of curing. The formulation design maintained fixed [$NO_3^-$]: [$OH^-$] ratios, therefore lower alkalinity generally resulted in

lower $NO_3^-$ concentration as well (Table 3). The XRD patterns show that the crystalline phase composition after a 3 month curing period is greatly dependent upon the activation solution alkalinity. Diffraction peaks assigned to zeolite X, zeolite P, and a chabazite phase (according to the peak at 2θ = 9.33°), were observed in the diffraction pattern of the sample prepared using the activation solution of lowest alkalinity (FA1-27.50d-0.5N). The same phases were observed in nitrate-free systems at the same alkalinity (FA1-27.50d-0N, **Fig. 6**). The intensity of the peaks attributed to zeolite X is higher than the intensity of peaks attributed to zeolite P, whereas the opposite was observed for the parallel nitrate-free geopolymer FA1-27.50d-0N. Peaks attributed to nitrate-bearing phases were not identified among the crystalline products formed at this alkalinity. Two wide humps, with maxima at 2θ ≈ 16° and 2θ ≈ 30°, can also be seen in the pattern. The dominance of these amorphous humps indicates a relatively high content of the neo-formed amorphous phase at these conditions.

Diffraction peaks corresponding to nitrate cancrinite were clearly observed in the diffraction patterns of samples FA1-13.75-1N and FA1-9.15d-1.4N, together with peaks corresponding to zeolite X. A single wide hump centered at 2θ ≈ 30° was observed in these samples, representing the amorphous phase. This hump is less dominant than those observed at lower alkalinity (FA1-27.50d-0.5N), indicating a higher degree of crystallinity at higher alkalinity. Increasing the nitrate content at $d$ = 9.15 had no impact on the nature of the crystalline phase as the diffraction pattern of FA1-9.15d-4.0N sample (not shown) was similar to the pattern of FA1-9.15d-1.4N sample.

**Figure 13** presents the corresponding FTIR spectra. The maximum intensity of the T-O-T asymmetric vibration absorbance band shifts to higher wavenumbers as the alkalinity and the nitrate concentration increase, (shifting from 985 $cm^{-1}$ for the FA1-27.50d-0.5N sample to 995 $cm^{-1}$ for FA1-9.15d-4.0N **Fig. 13A**), thus indicating a lower degree of Al incorporation within the geopolymer phase as the alkalinity and nitrate concentration increase. This trend is however reversed at highest alkalinity, where the maximal intensity of the asymmetric vibrations appeared at 987 $cm^{-1}$ (FA1-5.50d-2.5N samples, **Fig. 10**), despite the higher concentration of nitrate (2.5M). We may therefore conclude that both the alkalinity and the nitrate concentration have an impact on the geopolymerization processes in FA-based geopolymers. While the former has a promoting impact, enhancing both the dissolution and the condensation processes, as indicated by FTIR spectra of nitrate-free geopolymers (see **Fig. 7**), the later has an inhibiting impact in FA-based geopolymers, possibly interfering with the condensation and rearrangement processes.

This hypothesis is further supported by the vibrations of terminal T-OH groups in 830–880 $cm^{-1}$ range of the FTIR spectra (Fig. 13A), where two well-resolved absorbance bands appear after 3 months of curing only in FA1-9.15d-4.0N sample (at 835 $cm^{-1}$ and 865 $cm^{-1}$) while a single band at 873 $cm^{-1}$ with lower intensity appears in samples with lower nitrate content.

The 1200–1500 $cm^{-1}$ range of the FTIR spectra (Fig. 13B) which includes the N-O vibration bands yielded data that are in agreement with the XRD data. The most dominant band in all spectra was observed at 1383 $cm^{-1}$, in agreement with the spectra of samples prepared at higher alkalinity (see

Fig. 10). The band due to nitrate cancrinite (at 1423 $cm^{-1}$) was not observed for the FA1-27.50d-0.5N sample but was observed in samples activated at *d* = 13.75 and *d* = 9.15. The increase in the intensity of this band with increasing alkalinity is very minor, unlike the observations in MK-based geopolymers [17]. A higher nitrate content (FA1-9.15d-4.0N sample), where the $NaNO_3$ precursor is in excess did not lead to an increase in intensity of 1423 $cm^{-1}$ band (Fig. 13) demonstrating once again the inhibiting effect of nitrate ions on FA geopolymerization.

The absorbance at the SBU region of the FTIR spectra (Fig. 13A) reveals a band at 730 $cm^{-1}$ which is attributed to D6R rings present in zeolites such as chabazite and zeolite X. A band at 685 $cm^{-1}$ due to D6R units in cancrinite [29], together with additional well-resolved peaks of nitrate-cancrinite at 570 and 620 $cm^{-1}$, are observed for samples activated at *d* = 9.15. Absorbance bands at ~ 1035 $cm^{-1}$ and ~ 1120 $cm^{-1}$, which were also previously attributed to nitrate-cancrinite (Table 4), are also observed in the spectra of FA1-9.15d samples.

# 3.3 Mechanical characterization

The main factor influencing the compressive strength of cementitious monoliths is the ratio between the water (or activating solution) and the amount of the binder added. The compressive strength of geopolymers is also greatly influenced by the rate of the geopolymerization reactions as well as by the nature of the phases developed ([15, 43]). The design of the current study, which aimed for predetermined $Na_2O$:$Al_2O_3$ ratios, lead to a high solution:solid ratios when activating solutions of lower alkalinity were used. As a result, the measured compressive strength of samples prepared using activating solutions at dilutions higher than *d* > 5.50 was low (around 2 MPa). Therefore, we present the compressive strength developed after different curing periods only for geopolymers activated using the most alkaline solutions (*d* = 5.50).

The development of compressive strength of nitrate-free matrices prepared from FA1 using activation solutions at the highest alkalinity (*d* = 5.50) is compared in **Fig. 14** to the parallel matrices prepared from MK [17]. The FA1-5.50d-0N geopolymers ($Na_2O$: $Al_2O_3$ = 1.00) did not solidify during the first 2 days of curing, whereas the corresponding MK-based systems attained strength values of 0.6 ± 0.1 MPa after 1 day of curing. This is despite the lower water:binder ratio in the FA-based geopolymers (water:binder ratio of 0.57 in FA-based geopolymers vs 0.85 in the MK-based geopolymers). In both systems, the compressive strength increased with the curing time. MK-based samples reached their maximum strength values after about 14 days, whereas the compressive strength of FA1-based geopolymers continued to increase throughout the 90-day curing period. The compressive strength values attained by FA1-based systems after 90-days of curing were higher than the maximal values obtained by MK-based geopolymers, probably due to the lower water: binder ratio used [2]. The nature of the various crystalline phases identified in the systems and the lower content of crystalline phases in FA-geopolymers may be additional causes to the difference in the compressive strength values between FA-based and MK-based geopolymers.

The presence of sodium nitrate had an impact on the development of compressive strength in FA1-geopolymers. Figure 15 displays the average compressive strength values of FA1-geopolymers activated with varying concentrations of sodium nitrate measured after 7, 14, 28, and 90 days of curing. While for each of the samples prepared from FA1 the compressive strength increased with time, a clear decrease in compressive strength with increasing $NaNO_3$ content was observed for these samples, as well as for samples prepared from FA2 and FA3 (see Table 5). This is in contrast to the trend observed in MK-based systems, where nitrate ions were shown to enhance the rate of geopolymer rearrangements and strength development [17]. The strength of FA-based geopolymers continued to develop during the entire curing period of 90 days. Furthermore, the compressive strength values of FA-based nitrate-bearing geopolymers were found to be lower than those for the parallel MK-based geopolymers, despite the lower water:binder ratio. The ensemble of results presented here suggests that the presence of $NaNO_3$ impedes the strength development in fly-ash based geopolymers.

Table 5
Compressive strength values in FA-based geopolymers after 28 days of curing at *d* = 5.50, different FA types

| Sample | LOI of the FA | $SiO_2$:$Al_2O_3$ (molar) ratio in FA | W:FA [g/g] | Compressive strength after 28 days [MPa] |
|---|---|---|---|---|
| FA1-5.50d-0N | 6.0% | 2.3 | 0.57 | 6.0 ± 0.9 |
| FA1-5.50d-2.5N | 6.0% | 2.3 | 0.57 | 4.0 ± 0.9 |
| FA2-5.50d-0N | 1.2% | 4.3 | 0.43 | 15.6 ± 1.6 |
| FA2-5.50d-2.5N | 1.2% | 4.3 | 0.43 | 6.9 ± 1.4 |
| FA3-5.50d-0N | 2.4% | 4.6 | 0.43 | 11.5 ± 2.8 |
| FA3-5.50d-2.5N | 2.4% | 4.6 | 0.43 | 10.4 ± 4.0 |

# Discussion

The effect of nitrate ions on formation of FA-based geopolymers was studied by comparing the structural transformations within nitrate-free and nitrate-bearing matrices over a period of three months. Special attention was given to the formation of crystalline zeolites and feldspathoids, as these were recognized as potential immobilization sites for hazardous species present in industrial or nuclear waste streams [12, 13, 40, 44–50]. The results were compared to those obtained previously for metakaolin-based geopolymers [17].

Generally, the reorganization rate in FA-based geopolymers, as well as the content of the neo-formed crystalline phases, were found to be lower than in MK-based geopolymers, in agreement with previous findings [16, 51]. Furthermore, the nature of the minerals formed in nitrate-free FA-based geopolymers studied here differed from those formed in similar MK-based geopolymers [17]. Nitrate cancrinite was, however, the main crystalline phase obtained in nitrate-bearing geopolymers prepared from either FA or MK.

Unlike metakaolin, which is an amorphous alumino-silicate source containing only trace amounts of crystalline impurities, fly-ashes have a relatively high amount of crystalline content, and consequently a lower fraction of amorphous phase available for geopolymerization [16, 51]. This was found to have a profound effect on the resulting geopolymer matrices.

Quartz ($SiO_2$) and mullite ($Al_{1.83}Si_{1.08}O_{4.85}$) are two of the crystalline phases found often in raw fly-ashes [37, 52]. These phases do not undergo dissolution in alkaline media and therefore remain unaltered in the resulting geopolymeric products [16]. Rietveld analyses of diffraction patterns of samples prepared from FA1 and FA2 at *d* = 9.15 following 1 month of curing (Table 6, patterns not shown) indicate that the FA1-9.15*d*-1.4N sample contained 34 ± 4% and 6 ± 1% by weight of mullite and quartz, respectively, and FA2-9.15*d*-1.4N sample contained 17 ± 1% and 12 ± 1% by weight of mullite and quartz, respectively. The lower availability of an amorphous phase in FA in general is probably the main factor leading to the lower content of neo-formed crystalline phases in FA-based geopolymer matrices compared with similar MK-based geopolymers.

More specifically, the data presented in Table 6 indicates that the content of the amorphous phase available for geopolymerization in FA1 is lower than in FA2. This is also reflected in the measured pozzolanity values of these two fly-ashes, as shown in Table 2. Consequently, lower compressive strength was attained by FA1-based geopolymers compared to their FA2-based counterparts. The impact of the pozzolanity of the FA used is also reflected by the higher content of crystalline phases developed in the FA2-9.15*d*-1.4N geopolymers compared to the FA1-9.15*d*-1.4N (Table 6).

The amorphous phase availability in the precursor influences not only the properties of the final product but also the kinetics of the geopolymerization processes. FTIR analysis indicated that the rearrangements within the geopolymeric backbone of FA-based geopolymers studied here were still in progress after 3 months of curing at 40℃, unlike similar MK-based systems where indications of reorganization processes were no longer observed at this time. The lower geopolymerization rate in FA-based systems resulted in slower compressive strength development than in MK-based geopolymers [17]. Differences in morphology and surface area between FA and MK (BET values of 15 $m^2/g$ and 23 $m^2/g$, respectively) may also contribute to the lower rates of geopolymer formation and rearrangements. Furthermore, a setting of the neo-formed products on the surface of the spherical FA particles [35] can impede further product evolution, whereas full dissolution is usually obtained for MK platelets [17, 51].

Table 6
Quantitative Rietveld analysis of FA-based and MK-based geopolymers at *d* = 9.15 in presence of nitrate, after 1 month curing

| Sample name | Quartz | Mullite | Calcite | Anatase | Neo-formed crystalline phases | Amorphous phase |
|---|---|---|---|---|---|---|
| FA1-9.15*d*-1.4N | 6 ± 1% | 34 ± 4% | 1 ± 1% | — | 27 ± 4% | 32% |
| FA2-9.15*d*-1.4N | 12 ± 1% | 17 ± 1% | 1 ± 1% | — | 42 ± 4% | 28% |
| MK-9.15*d*-1.4N | 3 ± 2% | — | — | 2 ± 1% | 70 ± 4% | 25% |

The lower availability of amorphous phase in raw FA also leads to lower neo-formed crystalline content in FA-based geopolymer matrices compared with similar MK-based geopolymers (Table 6). The low resolution of absorbance bands in the SBU region of FTIR spectra, together with low signal/noise in XRD patterns of FA-based geopolymers are additional observations supporting this statement. In addition, due to the high mullite content in raw FA1, the $SiO_2$:$Al_2O_3$ ratio in the phases available for geopolymerization was probably higher than the nominal ratio indicated by the chemical analysis ($SiO_2$:$Al_2O_3$ = 2.3), as well as the ratio in raw MK ($SiO_2$:$Al_2O_3$ = 2.0). The extent of zeolite formation within geopolymer matrices is known to depend upon the $SiO_2$:$Al_2O_3$ ratio within the geopolymer mix. High $SiO_2$:$Al_2O_3$ ratios generally lead to the formation of highly amorphous materials, whereas lower ratios are more likely to result in the formation of crystalline zeolite domains embedded within the continuous amorphous geopolymer phase [15, 16]. The availability of silica and alumina species during geopolymer formation is in turn related to the composition and pozzolanity of the alumino-silicate source used, and to its dissolution rate which is also dependent upon the alkalinity of the activating solution [39, 53].

The alkalinity of the activation solution also has a great impact on the dissolution rate of the raw materials, which in turn affects the composition of the pore solution, the kinetics of the polymerization process, and the nature of the resulting products. It is well established that the dissolution rate of aluminum species from alumino-silicate materials is higher than that of silica species [17, 53]. At high alkalinity (*d* = 5.50), the alumina concentration in the pore solution increases at a higher rate than does the silica concentration, therefore the $SiO_2$:$Al_2O_3$ ratio becomes relatively low. These conditions are preferable for the formation of chabazite [37], which was found to be the dominant crystalline product in FA-based nitrate-free systems at *d* = 5.50. The formation of chabazites was previously reported in alkali-activated FA at higher temperatures than those used in the current study [14, 37, 44]. At lower alkalinities zeolites X and P were also obtained, in agreement with previous data [36, 40, 54–57]. This may be the result of the lower dissolution rate of the alumino-silicate materials at lower alkalinity (*d* > 5.50), which may have led to higher $SiO_2$:$Al_2O_3$ ratios which are known to promote the formation of zeolites P and X are preferable over the formation of other zeolites [34, 58].

Zeolite X is considered to be metastable with respect to zeolite P ([56, 59]) and chabazite [60] and is often obtained at lower $SiO_2$:$Al_2O_3$ ratios in the pore solution [55]), whereas zeolite P is obtained when this ratio is higher ([40, 55, 61]). The formation of zeolite X as the initial crystalline phase formed within geopolymer matrices was previously observed in low-silica MK-based geopolymers, where it was found to be metastable with respect to zeolite A [17]. Zeolite X is also reported to be the main crystalline phase in MK-based geopolymers cured at room temperature [62]. It is therefore suggested that zeolite X is the first crystalline phase formed in FA-based geopolymers as well, and this specific zeolite phase obtained following rearrangements within the geopolymer matrix depends upon the $SiO_2$:$Al_2O_3$ ratio within the geopolymer pore solution.

The presence of nitrate was found to delay the geopolymerization processes in FA-based samples, as evidenced by the SEM, FTIR, and compressive strength measurements. In MK-based systems investigated in a previous study [17], an opposite trend was observed. As discussed above, the reactive phase content in FA is lower in comparison to MK, and therefore the concentration of the dissolved monomers is lower than in MK-based geopolymers. Based on the results obtained in this study it may be suggested that nitrate anions interfere with monomer condensation stage and the geopolymer formation in these conditions. In contrast, in the more reactive MK, the concentration of the aluminate and silicate monomers may be sufficiently high in order to overcome such interferences, and therefore the condensation stage is not affected by the presence of the nitrates. In MK-containing geopolymers nitrate interference becomes dominant only at higher nitrate concentrations ([18, 23]).

The presence of nitrate ions did not alter the nature of the crystalline phases formed at the lowest alkalinity studied (at $d = 27.50$). At higher alkalinities, and consequently higher nitrate concentrations (> 2M $OH^-$ and > 0.5M $NO_3^-$), the nitrate-bearing feldspathoid, nitrate-cancrinite, was detected. This was true for all three fly ashes examined in this study, regardless of their chemical and physical properties, as well as for similar MK-based geopolymers [17]. The content of nitrate cancrinite in FA-based systems was lower than in MK-based geopolymers according to XRD and FTIR analysis. It is interesting to note that nitrate-sodalite, a precursor of nitrate cancrinite that was observed in MK-based geopolymers, could not be clearly identified in FA-based samples at similar alkalinities. We suggest that the low availability of alumina may have contributed to this observation, as the consequent high $Na_2O$:$Al_2O_3$ ratios during the condensation stages of FA-based geopolymers were shown to enhance the formation of nitrate-cancrinite [17].

Both cancrinite and chabazite formed in FA-based geopolymers at high alkalinity belong to the ABC-6 family of minerals [63]. These minerals have a common structural feature of 6-membered rings of silica and alumina tetrahedra, but differ in the relative position of the layers with respect to each other, leading to different sized cages and channels within the crystalline structure. The layers in cancrinite are arranged in an AB sequence, while chabazite is characterized by a double-layer stacking sequence of AABBCC [34, 63]. The review by Bonaccorsi and Merlino shows that the presence of different extra-framework anions such as chlorides, sulfates, carbonates and nitrates determine the stacking sequence

[63]. The findings in the current research further support this generalization. Nitrate was found to be a strong directing ion towards the cancrinite structure, while chabazite was observed in its absence. Minerals with the simple AB stacking sequence, such as cancrinites, may host the greatest amount of extra-framework anions [63].

The nature and the stability of the crystalline phases obtained will further influence the binding modes of hazardous species from various waste streams and the efficiency of their immobilization in the phases formed. For example, in presence of nitrate, zeolite X which is the initial crystalline phase formed at low alkalinities is metastable with respect to zeolite P [59], while the latter has a higher CEC (Cation Exchange Capacity) [58] and, therefore, a higher potential to incorporate cations of interest, such as hazardous metals and radionuclides. Chabazite was shown to be a good sorption medium for hazardous species ([7, 10, 50, 60, 64]). The nitrate-cancrinite was shown to have a high immobilization efficiency towards Cs, a radionuclide often found in low-level radioactive wastes [13, 63]. By controlling the various factors during the activation of FA or MK, one can tailor the geopolymeric product towards the formation of a specific mineral assemblage.

# Summary And Conclusions

This research examines some of the factors influencing the formation of different crystalline phases in FA-based geopolymers. Pozzolanity of the precursor, its morphology, the $SiO_2$: $Al_2O_3$ ratio of the initial amorphous phase and the alkalinity of the activation solution affect the $SiO_2$:$Al_2O_3$ ratio in the pore solution of the forming geopolymer, and thus, the nature of the zeolite formed. In nitrate-free systems, the nature of the minerals formed in the FA-based geopolymers included Na-Chabazite, zeolite P, zeolite X, and tobermorite. Nitrate-cancrinite was the dominant phase formed in the presence of nitrate at sufficiently high alkalinity in systems synthesized from both metakaolin and fly-ash, irrespective of variation in their physical and chemical properties. The formation of crystalline phases in FA-based geopolymers suggests that these materials may be used for immobilizing various hazardous species, while FA-based geopolymers containing the nitrate-cancrinite can be considered as a promising candidate for immobilizing Cs from radioactive wastes.

# Declarations

**Funding** (information that explains whether and by whom the research was supported)

The research was supported by the Pazy Foundation and by the Technion- Israel Institute of Technology.

### Conflicts of interest/Competing interests

The authors declare that they have no known competing financial interests or personal relationships that could have appeared to influence the work reported in this paper. Furthermore’ The authors have no financial or proprietary interests in any material discussed in this article.

**Availability of data and material** (data transparency)

Not applicable

**Code availability** (software application or custom code)

Not applicable

**Authors' contributions**

**Ela Ofer-Rozovsky:** Conceptualization, Methodology, Validation, Formal analysis, Investigation, Writing - Original Draft, Visualization

**Gabriela Bar-Nes:** Conceptualization, Methodology, Validation, Writing - Review & Editing, Funding acquisition

**Amnon Katz:** Conceptualization, Methodology, Validation, Resources, Writing - Review & Editing, Supervision, Project administration, Funding acquisition

**Michal Arbel-Haddad:** Conceptualization, Methodology, Validation, Writing - Original Draft, Writing - Review & Editing, Supervision, Project administration, Funding acquisition

**Ethics approval** (include appropriate approvals or waivers)

Not applicable

**Consent to participate** (include appropriate statements)

I'll be happy to participate as a reviewer of works in my field.

**Consent for publication**

I would like to publish the current article in Open Access.

**Acknowledgments.** The authors warmly acknowledge partial funding from the Pazy Foundation research no. 162 and from the Rieger Foundation- Jewish National Fund Program for Environment Studies.

# References

[1] J. Davidovits, Geopolymers: Inorganic polymeric new materials, J. Therm. Anal. 37 (1991) 1633–1656.

[2] P. Duxson, A. Fernandez-Jimenez, J.L. Provis, G.C. Lukey, A. Palomo, J.S.J. Deventer, Geopolymer technology: the current state of the art, J. Mater. Sci. 42 (2007) 2917–2933. https://doi.org/10.1007/s10853-006-0637-z.

[3] M. Grant Norton, J.L. Provis, 1000 at 1000: Geopolymer technology—the current state of the art, J. Mater. Sci. 55 (2020) 13487–13489. https://doi.org/10.1007/s10853-020-04990-z.

[4] J. Wang, J.X. Wang, Q. Zhang, Y.X. Li, Immobilization of simulated low and intermediate level waste in alkali-activated slag-fly ash-metakaolin hydroceramics, Nucl. Eng. Des. 300 (2016) 67–73. https://doi.org/10.1016/j.nucengdes.2016.01.011.

[5] Q. Tian, S. Nakama, K. Sasaki, Immobilization of cesium in fly ash-silica fume based geopolymers with different Si/Al molar ratios, Sci. Total Environ. 687 (2019) 1127–1137. https://doi.org/10.1016/j.scitotenv.2019.06.095.

[6] J.G.S. Van Jaarsveld, J.S.J. Van Deventer, L. Lorenzen, Factors Affecting the Immobilization of Metals in Geopolymerized Flyash, Metall. Mater. Trans. B. 29 (1998) 283–291. https://doi.org/10.1007/s11663-998-0032-z.

[7] J. Zhang, J.L. Provis, D. Feng, J.S.J. van Deventer, Geopolymers for immobilization of Cr(6+), Cd(2+), and Pb(2+)., J. Hazard. Mater. 157 (2008) 587–98. https://doi.org/10.1016/j.jhazmat.2008.01.053.

[8] V. Nikolic, M. Komljenovic, N. Dzunuzovic, Z. Miladinovic, The influence of Pb addition on the properties of fly ash-based geopolymeres, J. Hazard. Mater. 350 (2018) 98–107. doi: 10.1016/j.jhazmat.2018.02.023.

[9] Q. Li, Z. Sun, D. Tao, Y. Xu, P. Li, H. Cui, J. Zhai, Immobilization of simulated radionuclide 133Cs+ by fly ash-based geopolymer, J. Hazard. Mater. 262 (2013) 325–331. https://doi.org/10.1016/j.jhazmat.2013.08.049.

[10] A. Fernández-Jiménez, D.E. Macphee, E.E. Lachowski, A. Palomo, Immobilization of cesium in alkaline activated fly ash matrix, J. Nucl. Mater. 346 (2005) 185–193. https://doi.org/10.1016/j.jnucmat.2005.06.006.

[11] K. Shiota, T. Nakamura, M. Takaoka, S. Aminuddin, K. Oshita, T. Fujimori, Stabilization of cesium in alkali-activated municipal solid waste incineration fly ash and a pyrophyllite-based system, Chemosphere. 187 (2017) 188–195.

[12] M. Arbel Haddad, E. Ofer-Rozovsky, G. Bar-Nes, E.J.C. Borojovich, A. Nikolski, D. Mogiliansky, A. Katz, Formation of zeolites in metakaolin-based geopolymers and their potential application for Cs immobilization, J. Nucl. Mater. 493 (2017) 168–179. https://doi.org/10.1016/j.jnucmat.2017.05.046.

[13] E. Ofer-Rozovsky, M. Arbel Haddad, G. Bar-nes, E.J.C. Borochovitz, A. Binyamini, A. Nikolski, A. Katz, Cesium immobilization in nitrate-bearing metakaolin-based geopolymers, J. Nucl. Mater. 514 (2019) 247–254. https://doi.org/10.1016/j.jnucmat.2018.11.003.

[14] P. Rozek, M. Krol, W. Mozgawa, Geopolymer-zeolite composites : A review, J. Clean. Prod. 230 (2019) 557–579. https://doi.org/10.1016/j.jclepro.2019.05.152.

[15] J.L. Provis, G.C. Lukey, J.S.J. Van Deventer, Do geopolymers actually contain nanocrystalline zeolites? a reexamination of existing results, Chem. Mater. 17 (2005) 3075–3085. https://doi.org/10.1021/cm050230i.

[16] A. Fernández-Jiménez, M. Monzo, M. Vicent, A. Barba, A. Palomo, Alkaline activation of metakaolin-fly ash mixtures: Obtain of Zeoceramics and Zeocements, Microporous Mesoporous Mater. 108 (2008) 41–49. https://doi.org/10.1016/j.micromeso.2007.03.024.

[17] E. Ofer-Rozovsky, M. Arbel Haddad, G. Bar-Nes, A. Katz, The formation of crystalline phases in metakaolin-based geopolymers in the presence of sodium nitrate, J. Mater. Sci. 51 (2016) 4975–4814. https://doi.org/10.1007/s10853-016-9767-0.

[18] C. Desbats-Le Chequer, F. Frizon, Impact of sulfate and nitrate incorporation on potassium- and sodium-based geopolymers: Geopolymerization and materials properties, J. Mater. Sci. 46 (2011) 5657–5664. https://doi.org/10.1007/s10853-011-5516-6.

[19] J.L. Bell, P. Sarin, J.L. Provis, R.P. Haggerty, P.E. Driemeyer, P.J. Chupas, J.S.J. van Deventer, W.M. Kriven, Atomic structure of a cesium aluminosilicate geopolymer: A pair distribution function study, Chem. Mater. 20 (2008) 4768–4776. https://doi.org/10.1021/cm703369s.

[20] J.L. Bell, P.E. Driemeyer, W.M. Kriven, Formation of ceramics from metakaolin-based geopolymers. Part II: K-based geopolymer, J. Am. Ceram. Soc. 92 (2009) 607–615. https://doi.org/10.1111/j.1551-2916.2008.02922.x.

[21] W.K. Lee, J.S.J. van Deventer, The effects of inorganic salt contamination on the strength and durability of geopolymers, Colloids Surfaces A Physicochem. Eng. Asp. 211 (2002) 115–126. https://doi.org/10.1016/S0927-7757(02)00239-X.

[22] K. Komnitsas, D. Zaharaki, G. Bartzas, Effect of sulphate and nitrate anions on heavy metal immobilisation in ferronickel slag geopolymers, Appl. Clay Sci. 73 (2013) 103–109. https://doi.org/10.1016/j.clay.2012.09.018.

[23] N.R. Rakhimova, R.Z. Rakhimov, Y.N. Osin, N.I. Naumkina, A.M. Gubaidullina, G.I. Yakovlev, A. V Shaybadullina, Solidification of nitrate solutions with alkali-activated slag and slag – metakaolin cements, J. Nucl. Mater. 457 (2015) 186–195. https://doi.org/10.1016/j.jnucmat.2014.11.068.

[24] G.W. Ware, Nitrate and Nitrite, in: Rev. Environ. Contam. Toxicol., Springer, NY, New York, 1989: pp. 117–130. https://doi.org/doi.org/10.1007/978-1-4684-7083-3.

[25] W. Kraus, G. Nolze, G. Federal Institute for Materials Research and Testing, Berlin, PowerCell version 2.4, (2000).

[26] A. Le Bail, Modeling the silica glass structure by the Rietveld method., J. Non. Cryst. Solids. 183 (1995) 39–42. https://doi.org/10.1016/0022-3093(94)00664-4.

[27] Pearson's Crystal Data: Crystal Structure Database for Inorganic Compounds (on CD-ROM), (2012).

[28] I. Ismail, S. Bernal, J. Provis, R. San Nicolas, S. Hamdan, J.S.J. van Deventer, Modification of phase evolution in alkali-activated blast furnace slag by the incorporation of fly ash, Cem. Concr. Compos. 45 (2014). https://doi.org/10.1016/j.cemconcomp.2013.09.006.

[29] J.C. Buhl, C. Taake, F. Stief, M. Fechtelkord, The crystallisation kinetics of nitrate cancrinite Na-7.6[AlSiO4](6)(NO3)(1.6) (H2O2)(2) under low temperature hydrothermal conditions, React. Kinet. Catal. Lett. 69 (2000) 15–21. https://doi.org/10.1023/A:1005676322206.

[30] A. Demortier, N. Gobeltz, J.P. Lelieur, C. Duhayon, Infrared evidence for the formation of an intermediate compound during the synthesis of zeolite Na–A from metakaolin, Int. J. Inorg. Mater. 1 (1999) 129–134. https://doi.org/10.1016/S1466-6049(99)00020-3.

[31] A. Fernández-Jiménez, A. Palomo, Mid-infrared spectroscopic studies of alkali-activated fly ash structure, Microporous Mesoporous Mater. 86 (2005) 207–214. https://doi.org/10.1016/j.micromeso.2005.05.057.

[32] M.C. Barnes, J. Addai-Mensah, A.R. Gerson, A methodology for quantifying sodalite and cancrinite phase mixtures and the kinetics of the sodalite to cancrinite phase transformation, 31 (1999) 303–319.

[33] J.C. Buhl, J. Lons, Synthesis and crystal structure of nitrate enclathrated sodalite Na-8[AlSiO4](6)(NO3)(2), J. Alloys Compd. 235 (1996) 41–47. https://doi.org/10.1016/0925-8388(95)02148-5.

[34] J.E. Oh, P.J.M. Monteiro, S.S. Jun, S. Choi, S.M. Clark, The evolution of strength and crystalline phases for alkali-activated ground blast furnace slag and fly ash-based geopolymers, Cem. Concr. Res. 40 (2010) 189–196. https://doi.org/10.1016/j.cemconres.2009.10.010.

[35] A. Fernández-Jiménez, A. Palomo, M. Criado, Microstructure development of alkali-activated fly ash cement: A descriptive model, Cem. Concr. Res. 35 (2005) 1204–1209. https://doi.org/10.1016/j.cemconres.2004.08.021.

[36] C. a. Ríos R., C.D. Williams, C.L. Roberts, A comparative study of two methods for the synthesis of fly ash-based sodium and potassium type zeolites, Fuel. 88 (2009) 1403–1416. https://doi.org/10.1016/j.fuel.2009.02.012.

[37] J.E. Oh, Y. Jun, Y. Jeong, Characterization of geopolymers from compositionally and physically different Class F fly ashes, Cem. Concr. Compos. 50 (2014) 16–26. https://doi.org/10.1016/j.cemconcomp.2013.10.019.

[38] Z. Zheng, Y. Li, H. Sun, Z. Zhang, X. Ma, Coupling effect of NaOH and NaNO3 on the solidified fly ash-cement matrices containing Cs+: Reaction products, microstructure and leachability, J. Nucl. Mater. 539 (2020) 152252. https://doi.org/10.1016/j.jnucmat.2020.152252.

[39] H. Rahier, J. Wastiels, M. Biesemans, R. Willlem, G. Assche, B. Mele, G. Van Assche, B. Van Mele, Reaction mechanism, kinetics and high temperature transformations of geopolymers, J. Mater. Sci. 42 (2006) 2982–2996. https://doi.org/10.1007/s10853-006-0568-8.

[40] X. Querol, Synthesis of zeolites from coal fly ash: an overview, Int. J. Coal Geol. 50 (2002) 413–423. https://doi.org/10.1016/S0166-5162(02)00124-6.

[41] J.C. Buhl, F. Stief, M. Fechtelkord, T.M. Gesing, U. Taphorn, C. Taake, Synthesis, X-ray diffraction and MAS NMR characteristics of nitrate cancrinite Na-7.6[AlSiO4](6)(NO3)(1.6)(H2O)(2), J. Alloys Compd. 305 (2000) 93–102. https://doi.org/10.1016/S0925-8388(00)00724-6.

[42] A. Burton, M. Feuerstein, R.F. Lobo, J.C.C. Chan, Characterization of cancrinite synthesized in 1,3-butanediol by Rietveld analysis of powder neutron diffraction data and solid-state 23Na NMR spectroscopy, Microporous Mesoporous Mater. 30 (1999) 293–305. https://doi.org/10.1016/S1387-1811(99)00040-2.

[43] P. Rovnaník, Effect of curing temperature on the development of hard structure of metakaolin-based geopolymer, Constr. Build. Mater. 24 (2010) 1176–1183. https://doi.org/10.1016/j.conbuildmat.2009.12.023.

[44] A.R. Brough, A. Katz, G.K. Sun, L.J. Struble, R.J. Kirkpatrick, J.F. Young, Adiabatically cured, alkali-activated cement-based wasteforms containing high levels of fly ash Formation of zeolites and Al-substituted C-S-H, Cem. Concr. Res. 31 (2001) 1437–1447. https://doi.org/10.1016/S0008-8846(01)00589-0.

[45] J. Mon, Y. Deng, M. Flury, J.B. Harsh, Cesium incorporation and diffusion in cancrinite, sodalite, zeolite, and allophane, Microporous Mesoporous Mater. 86 (2005) 277–286. https://doi.org/10.1016/j.micromeso.2005.07.030.

[46] H.A. Ibrahim, A.M. El-Kamash, M. Hanafy, N.M. Abdel-Monem, Examination of the use of synthetic Zeolite NaA-X blend as backfill material in a radioactive waste disposal facility: Thermodynamic approach, Chem. Eng. J. 144 (2008) 67–74. https://doi.org/10.1016/j.cej.2008.01.012.

[47] S. Chen, M. Wu, S. Zhang, Mineral phases and properties of alkali-activated metakaolin-slag hydroceramics for a disposal of simulated highly-alkaline wastes, J. Nucl. Mater. 402 (2010) 173–178. https://doi.org/10.1016/j.jnucmat.2010.05.015.

[48] R.M. Barrer, Zeolites and Clay Minerals as Sorbents and Moleculer Sieves, Acadamic Press, London, New York, San Francisco, 1978.

[49] D.W. Breck, Zeolite Molecular Sieves: Structure, Chemistry and Use, New York, 1974.

[50] E.H. Borai, R. Harjula, L. Malinen, A. Paajanen, Efficient removal of cesium from low-level radioactive liquid waste using natural and impregnated zeolite minerals., J. Hazard. Mater. 172 (2009) 416–22.

https://doi.org/10.1016/j.jhazmat.2009.07.033.

[51] J.S.J. van Deventer, J. Provis, P. Duxson, G.C. Lukey, Reaction mechanisms in the geopolymeric conversion of inorganic waste to useful products., J. Hazard. Mater. 139 (2007) 506–13. https://doi.org/10.1016/j.jhazmat.2006.02.044.

[52] E.I. Diaz, E.N. Allouche, S. Eklund, Factors affecting the suitability of fly ash as source material for geopolymers, Fuel. 89 (2010) 992–996. https://doi.org/10.1016/j.fuel.2009.09.012.

[53] L. Weng, K. Sagoe-Crenstil, Dissolution processes, hydrolysis and condensation reactions during geopolymer synthesis: Part I—Low Si /Al ratio systems, J. Mater. Sci. 42 (2007) 2997–3006. https://doi.org/0.1007/s10853-006-0820-2.

[54] A. Katz, A.R. Brough, R.J. Kirkpatrick, L.J. Struble, G.K. Sun, J.F. Young, Cement solidification of simulated off-gas condensates from vitrification of low-level nuclear waste solutions, Waste Manag. 21 (2001) 543–553. https://doi.org/10.1016/S0956-053X(00)00105-7.

[55] H. Tanaka, S. Furusawa, R. Hino, Synthesis , Characterization , and Formation Process of Na – X Zeolite from Coal Fly Ash, J. Mater. 10 (2002).

[56] A. Molina, C. Poole, A comparative study using two methods to produce zeolites from fly ash, Amin. Eng. 17 (2004) 167–173. https://doi.org/10.1016/j.mineng.2003.10.025.

[57] A. Fernández-Jiménez, I. García-Lodeiro, A. Palomo, Durability of alkali-activated fly ash cementitious materials, J. Mater. Sci. 42 (2006) 3055–3065. https://doi.org/10.1007/s10853-006-0584-8.

[58] G.G. Hollman, G. Steenbruggen, M. Janssen-Jurkovičová, A two-step process for the synthesis of zeolites from coal fly ash, Fuel. 78 (1999) 1225–1230. https://doi.org/10.1016/S0016-2361(99)00030-7.

[59] C.W. Purnomo, C. Salim, H. Hinode, Synthesis of pure Na-X and Na-A zeolite from bagasse fly ash, Microporous Mesoporous Mater. 162 (2012) 6–13. https://doi.org/10.1016/j.micromeso.2012.06.007.

[60] L. Van Tendeloo, W. Wangermez, M. Kurttepeli, B. De Blochouse, S. Bals, G. Van Tendeloo, J.A. Martens, A. Maes, C.E.A. Kirschhock, E. Breynaert, Chabazite: Stable cation-exchanger in hyper alkaline concrete pore water, Environ. Sci. Technol. 49 (2015) 2358–2365. https://doi.org/10.1021/es505346j.

[61] Z. Zheng, X. Ma, Z. Zhang, Y. Li, In-situ transition of amorphous gels to Na-P1 zeolite in geopolymer: Mechanical and adsorption properties, Constr. Build. Mater. 202 (2019) 851–860. https://doi.org/10.1016/j.conbuildmat.2019.01.067.

[62] E. Ofer-Rozovsky, Solidification in Geopolymers of Low-Level Nuclear Waste Containing Cesium, Technion I.I.T, 2017.

[63] E. Bonaccorsi, S. Merlino, Modular microporous minerals: Cancrinite-davyne group and C-S-H phases, Rev. Mineral. Geochemistry. 57 (2005) 241–290. https://doi.org/10.2138/rmg.2005.57.8.

[64] J. Chorover, S. Choi, M.K. Amistadi, K.G. Karthikeyan, G. Crosson, K.T. Mueller, Linking cesium and strontium uptake to kaolinite weathering in simulated tank waste leachate.

# Figures

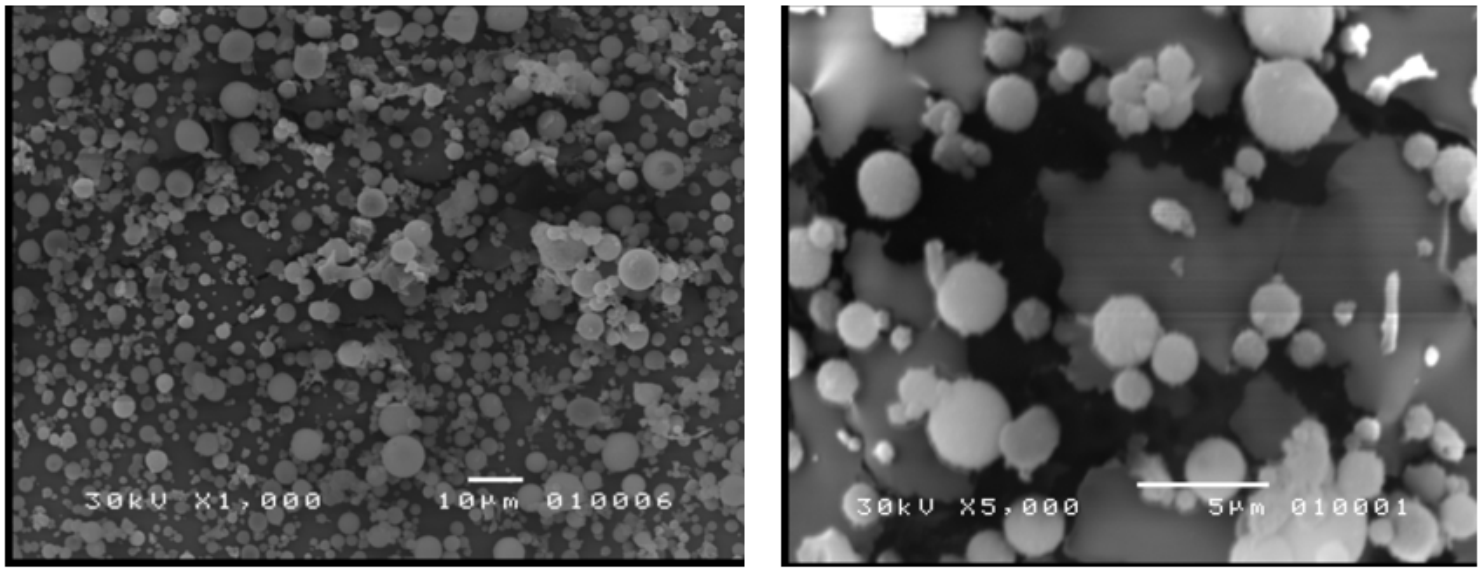


**Figure 1**

SEM images in SE mode of raw FA-1

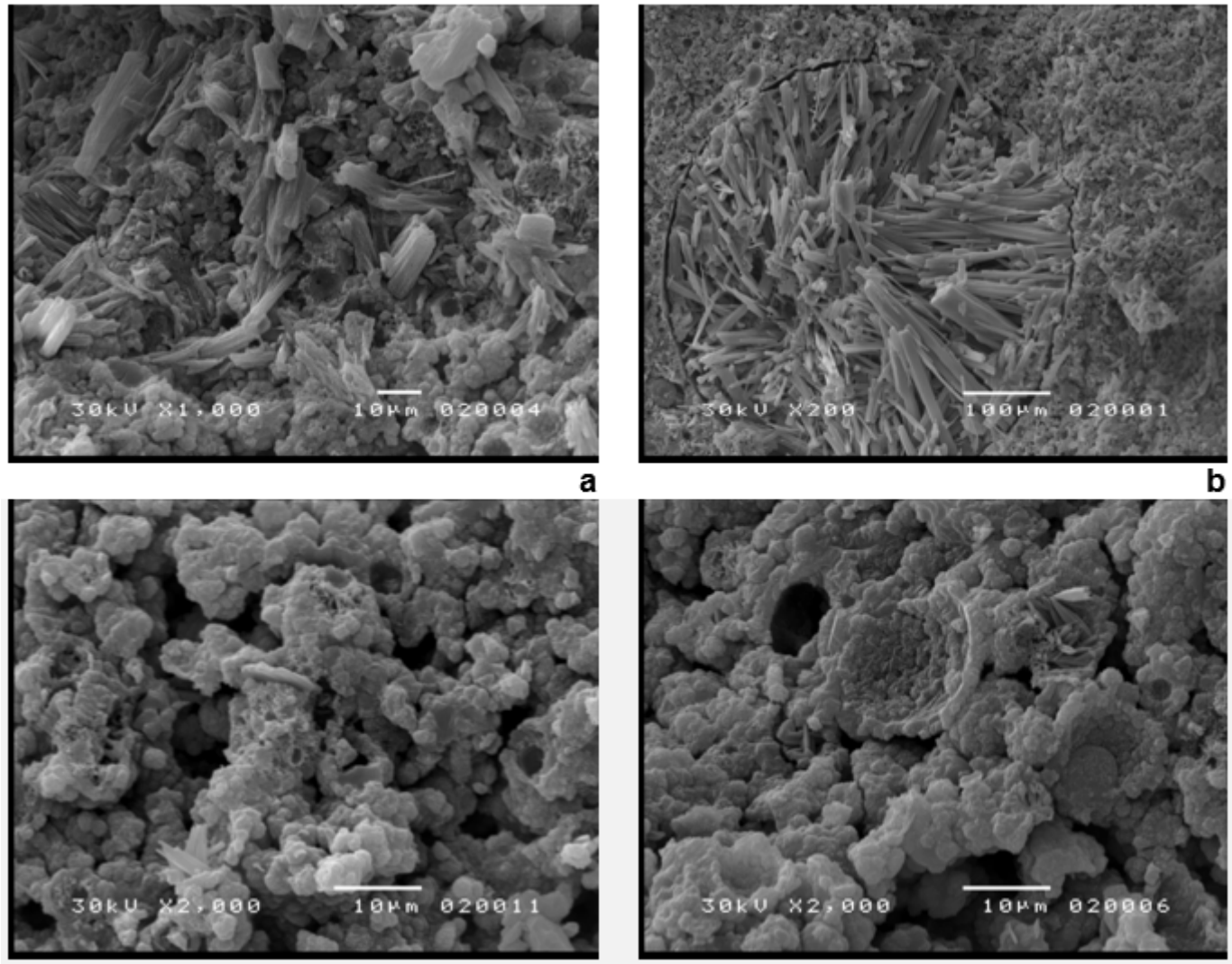


## Figure 2

SEM images in SE mode of FA1-5.50d-0N samples, 3 months curing

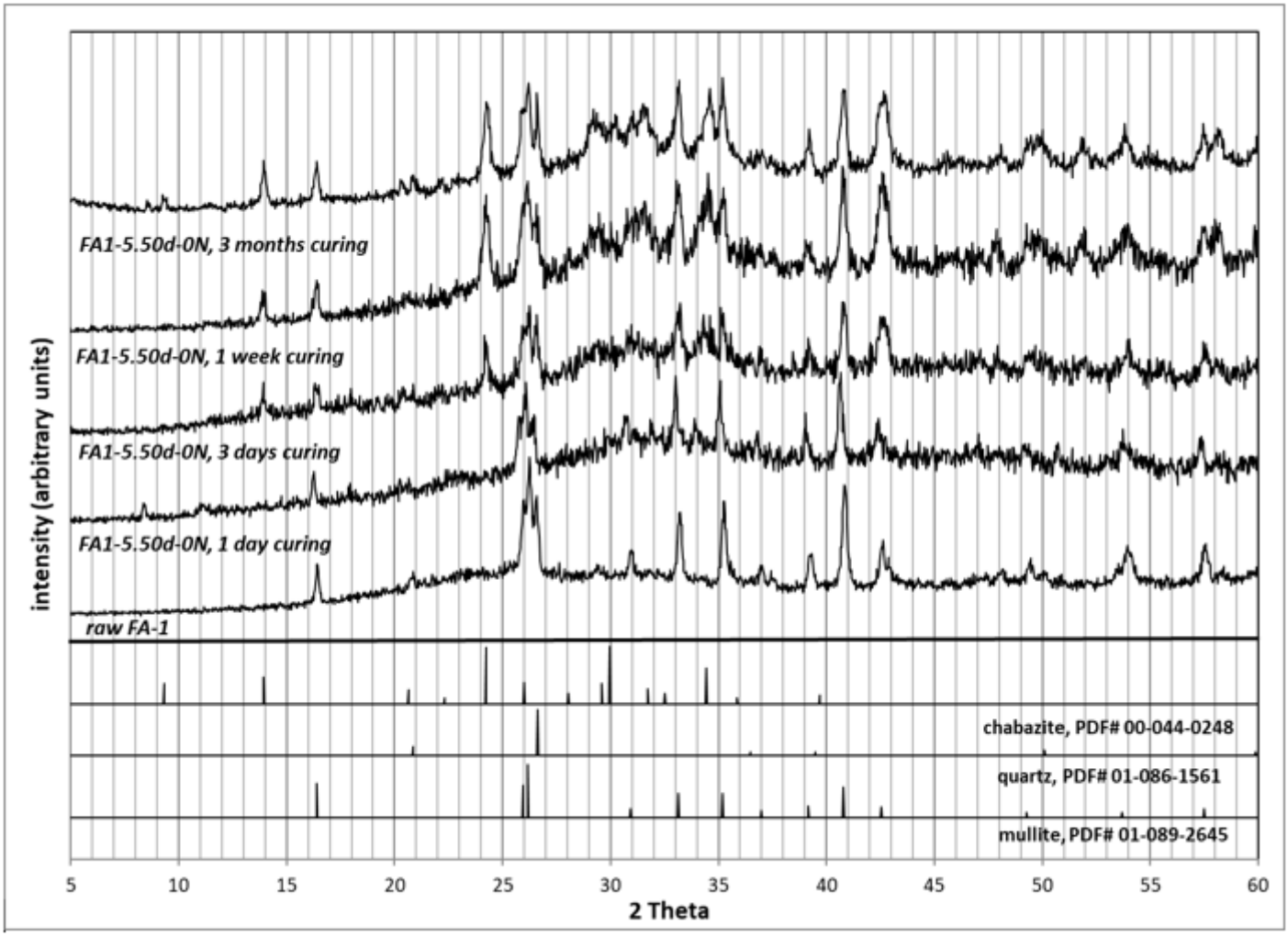


## Figure 3

XRD patterns of FA-1 and FA1-5.50d-0N samples for different curing times

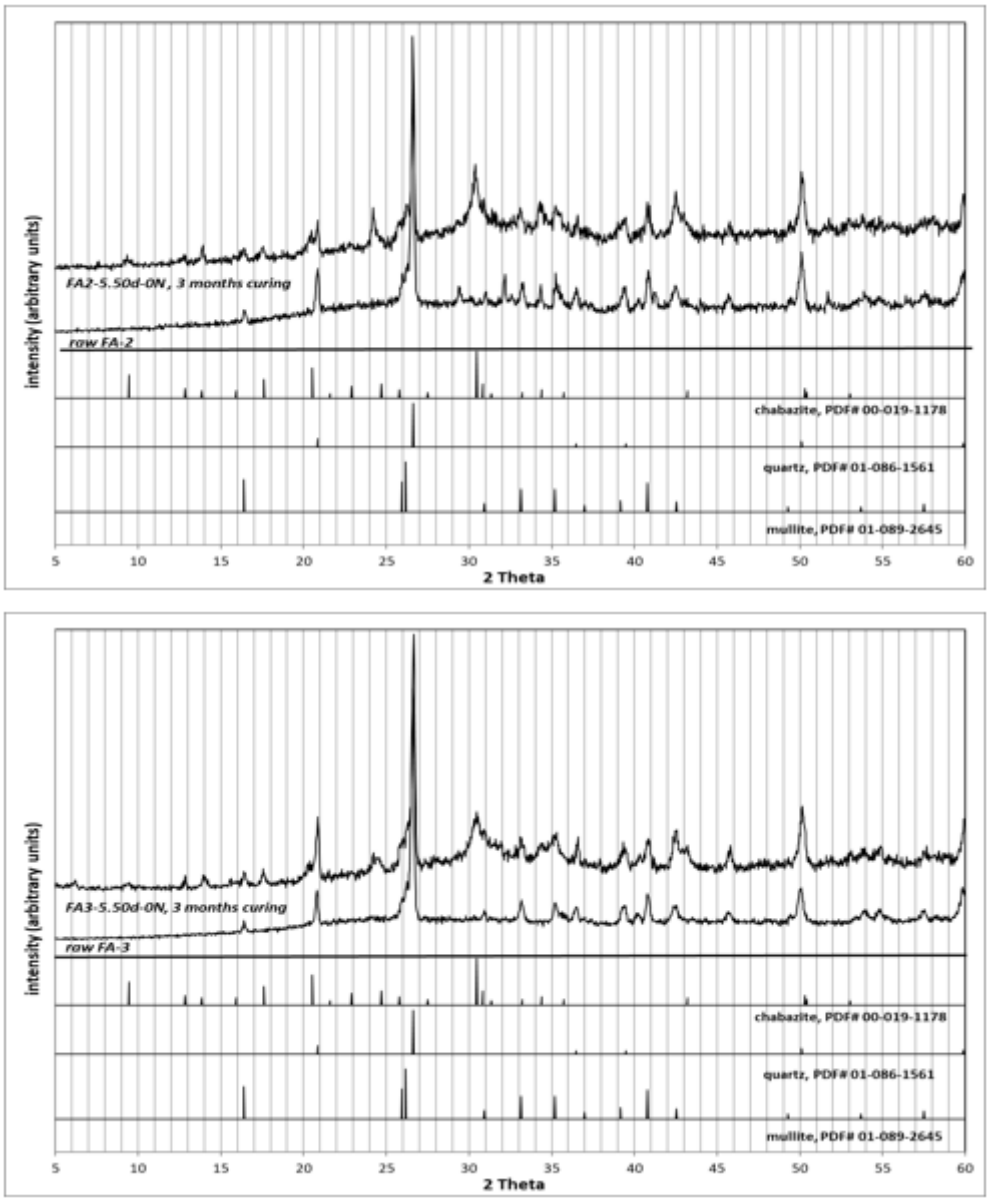


## Figure 4

XRD patterns of FA-2, FA-3, FA2-5.50d-0N and FA3-5.50d-0N samples, 3 months curing

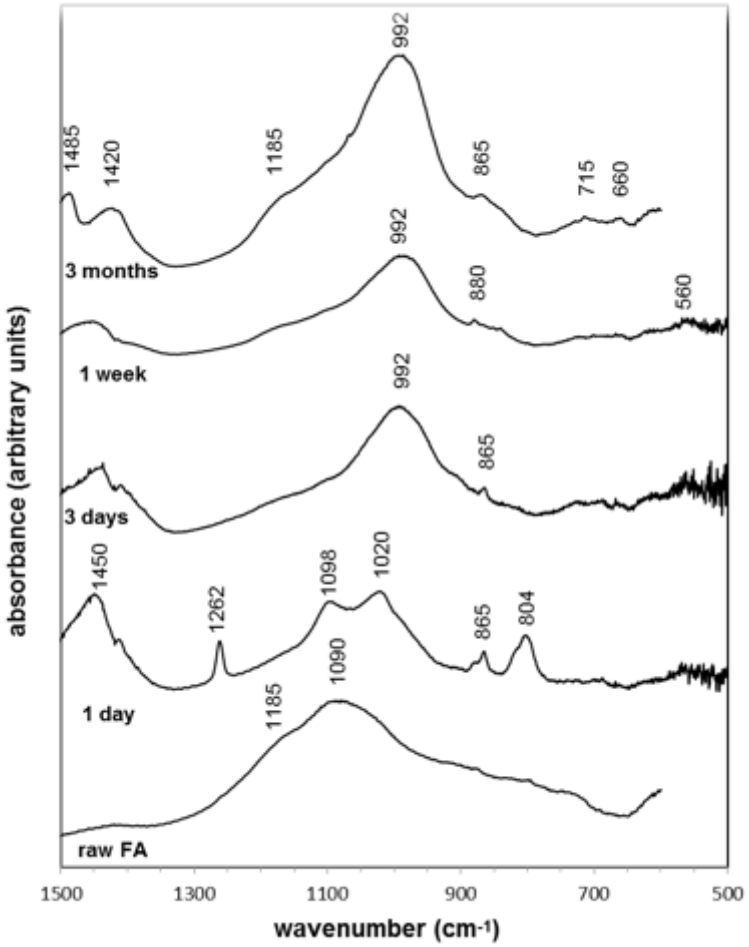


## Figure 5

FTIR spectra of FA-1 and FA1-5.50d-0N samples for different curing times

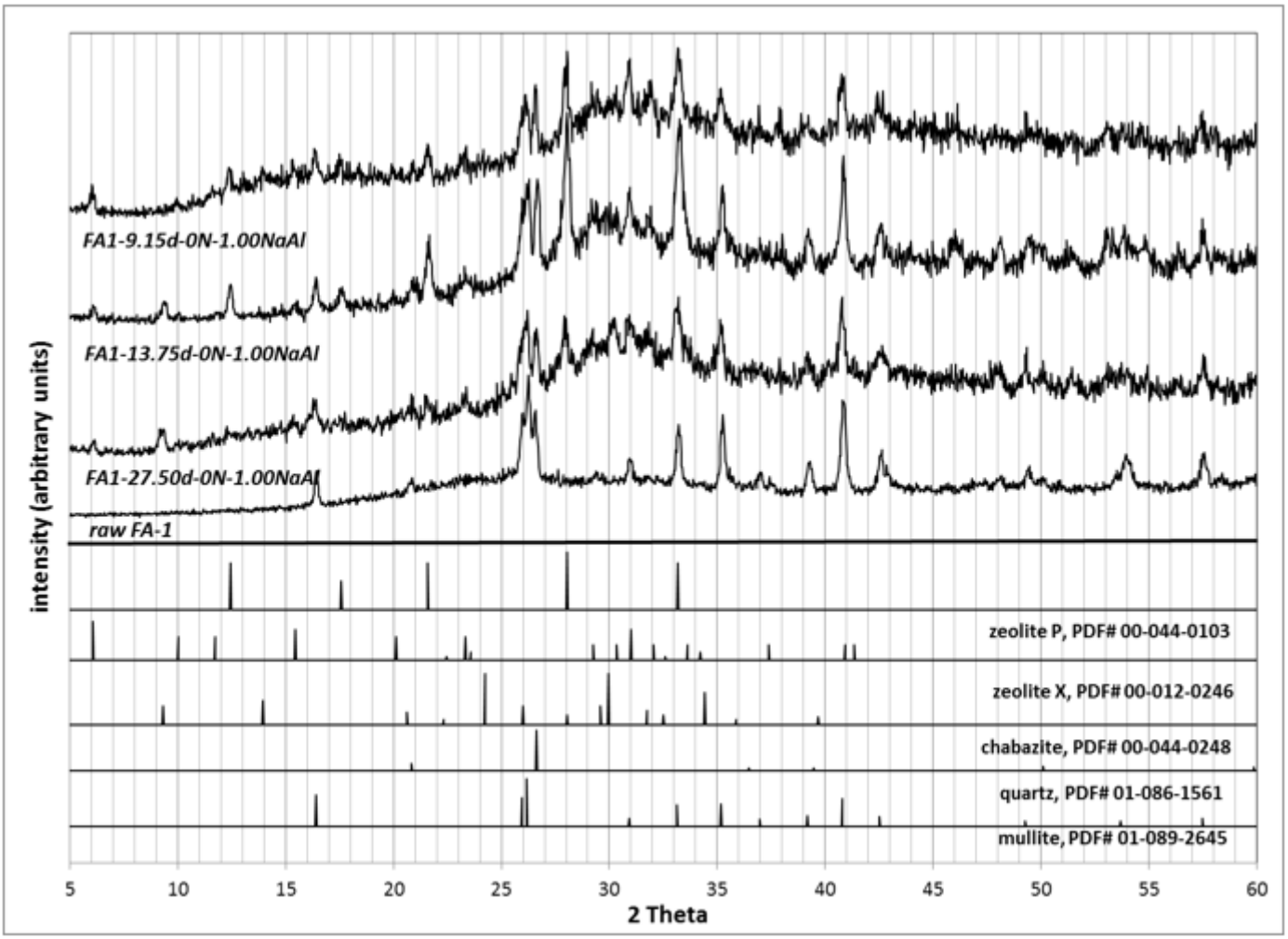


## Figure 6

XRD patterns of FA-1, FA1-9.15d-0N, FA1-13.75d-0N and FA1-27.50d-0N samples, 3 months curing

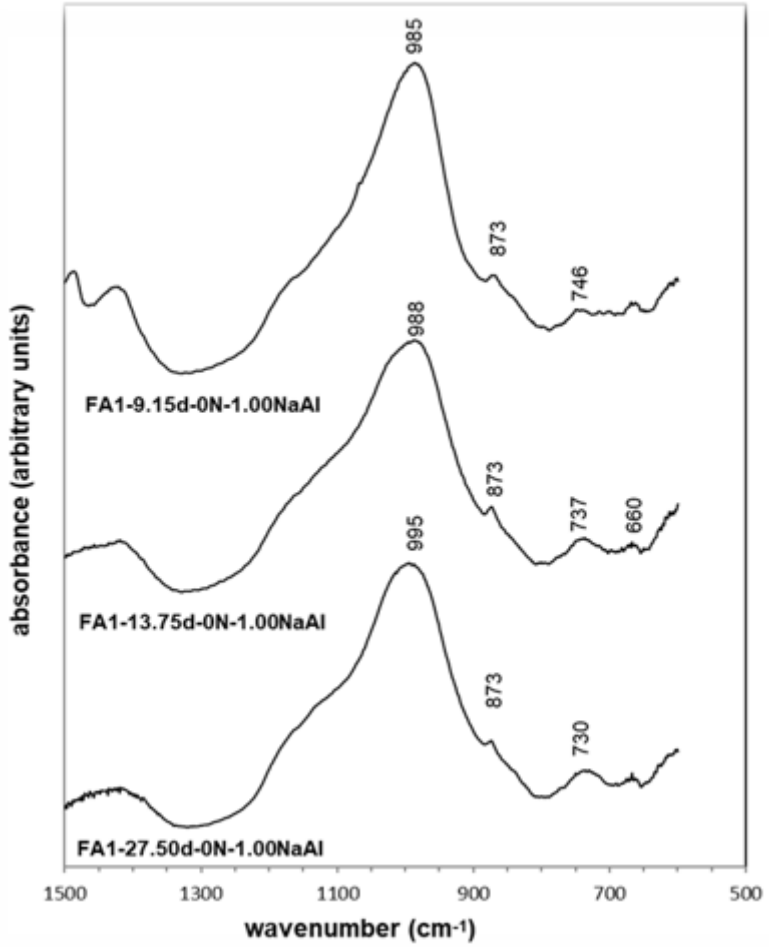


## Figure 7

FTIR spectra of FA-1, FA1-9.15d-0N, FA1-13.75d-0N and FA1-27.50d-0N samples, 3 months curing

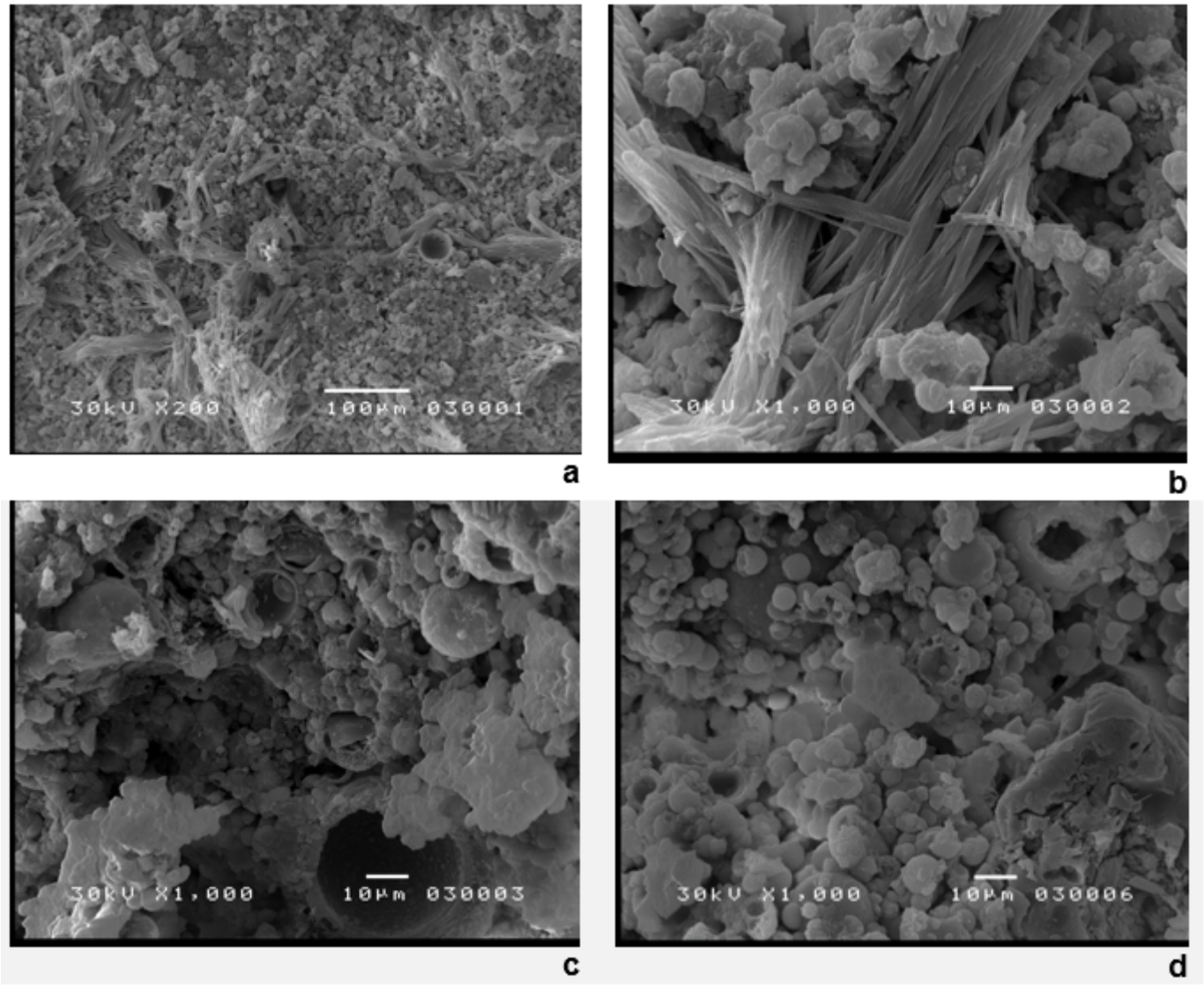


## Figure 8

SEM images in SE mode of FA1-5.50d-3.0N samples, 3 months curing

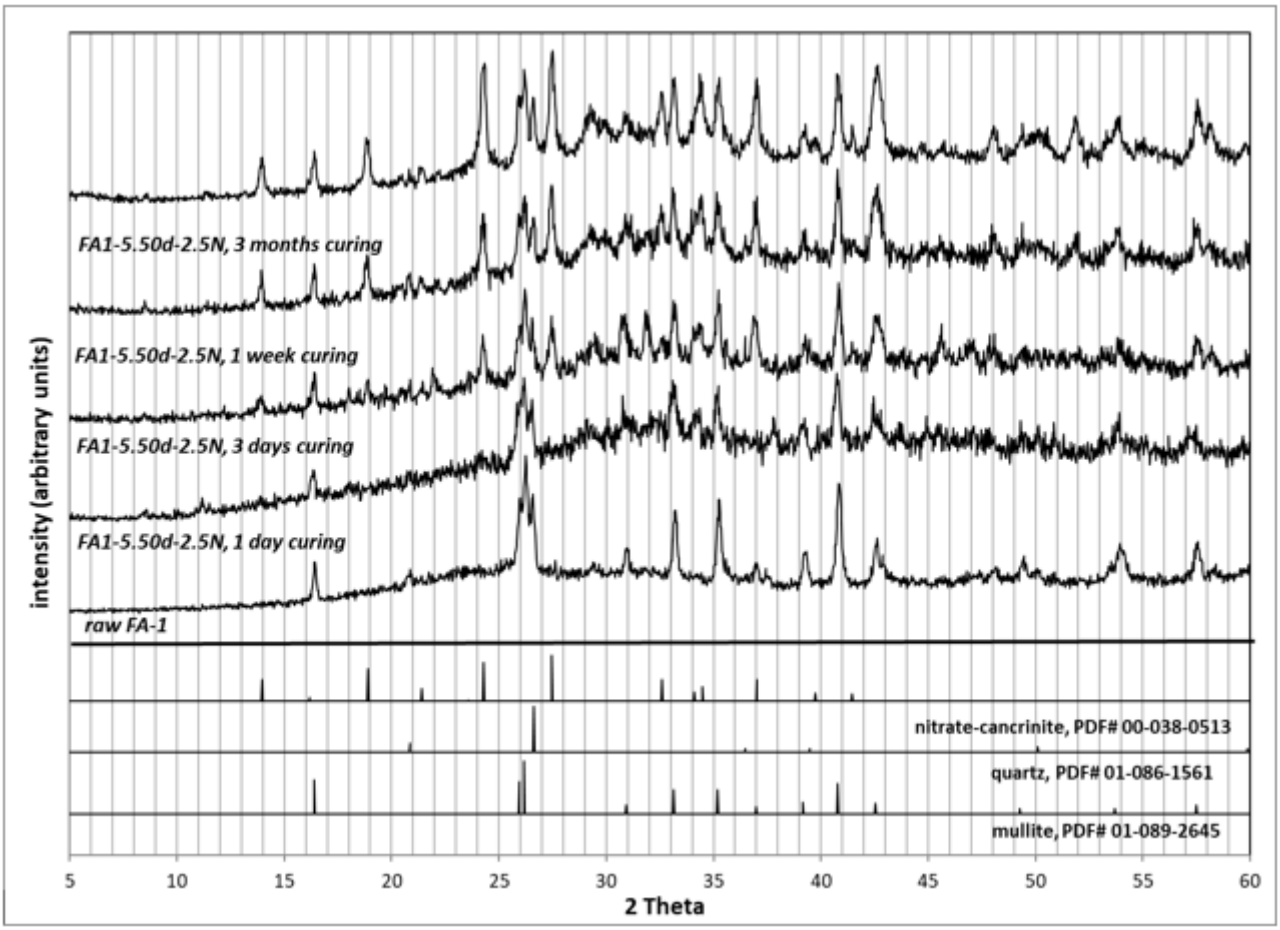


## Figure 9

XRD patterns of FA-1 and FA1-5.50d-2.5N samples for different curing times

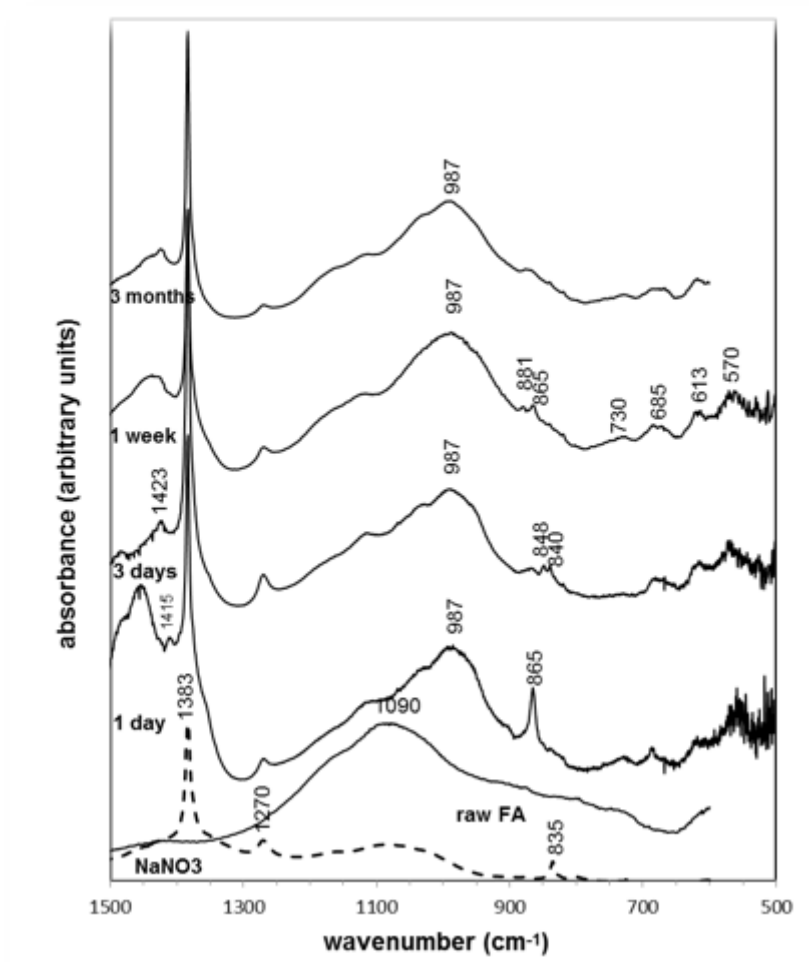


## Figure 10

FTIR spectra of FA-1 and FA1-5.50d-2.5N samples for different curing times

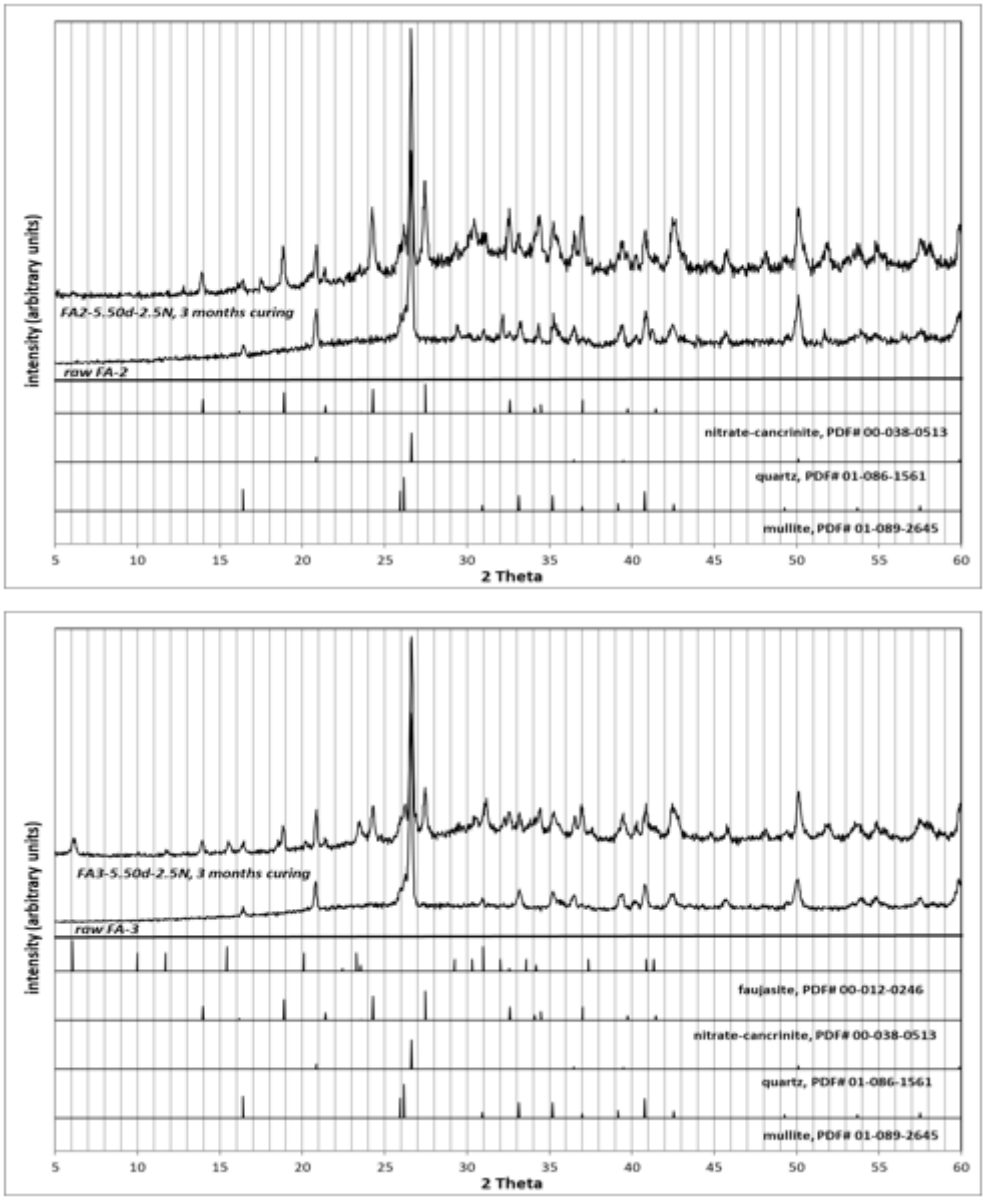


## Figure 11

XRD patterns of FA-2, FA-3, FA2-5.50d-2.5N and FA3-5.50d-2.5N samples, 3 months curing

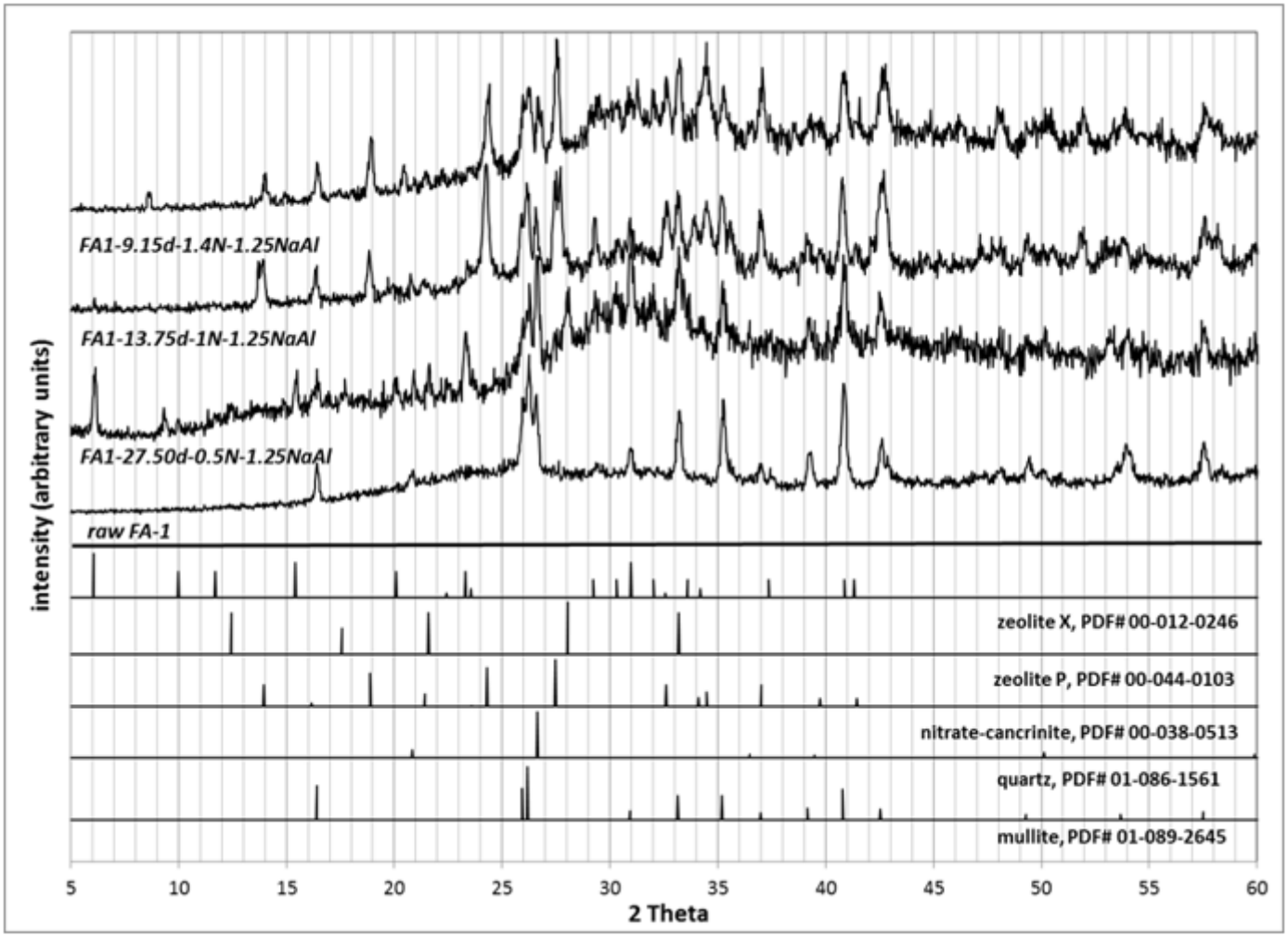


## Figure 12

XRD patterns of FA-1, FA1-9.15d-1.4N, FA1-13.75d-1.0N and FA1-27.50d-0.5N samples, 3 months curing

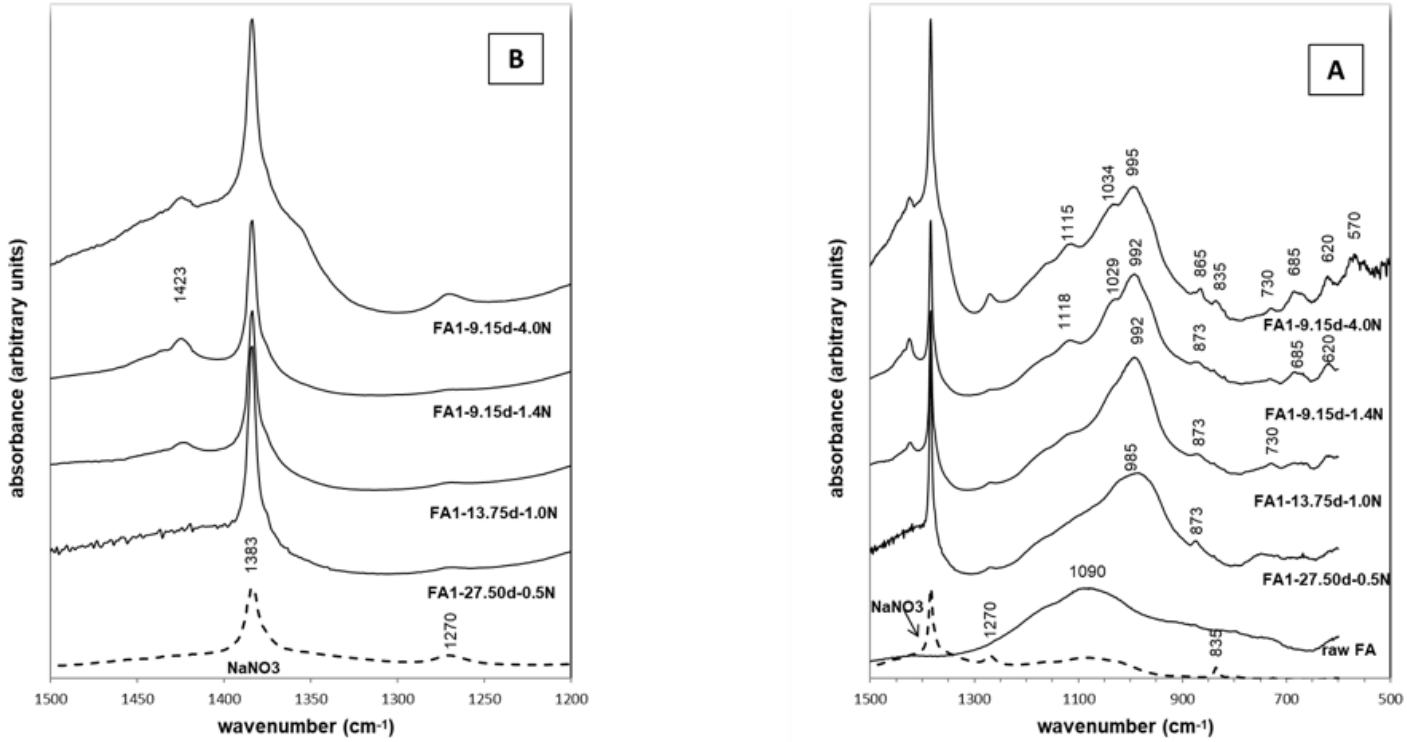


## Figure 13

FTIR spectra of FA-1, NaNO3, FA1-9.15d-4.0N, FA1-9.15d-1.4N, FA1-13.75d-1.0N and FA1-27.50d-0.5N samples, 3 months curing. 500-1500 cm-1 region (A) and zoomed 1200-1500 cm-1 region (B)

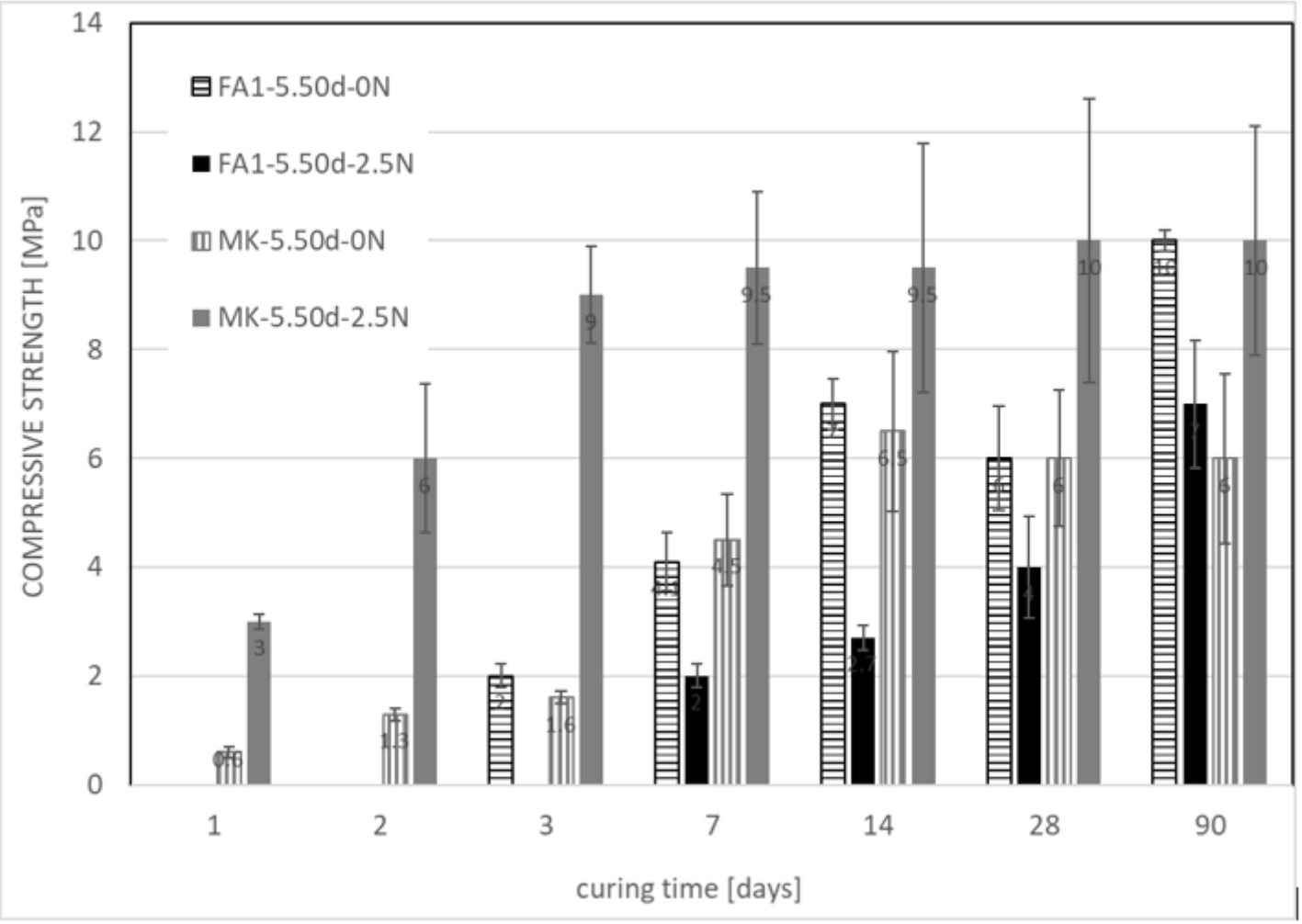


## Figure 14

Compressive strength development in FA1-based geopolymers and MK-based geopolymers during the curing at d=5.50 (W:FA=0.57, W:MK=0.85)

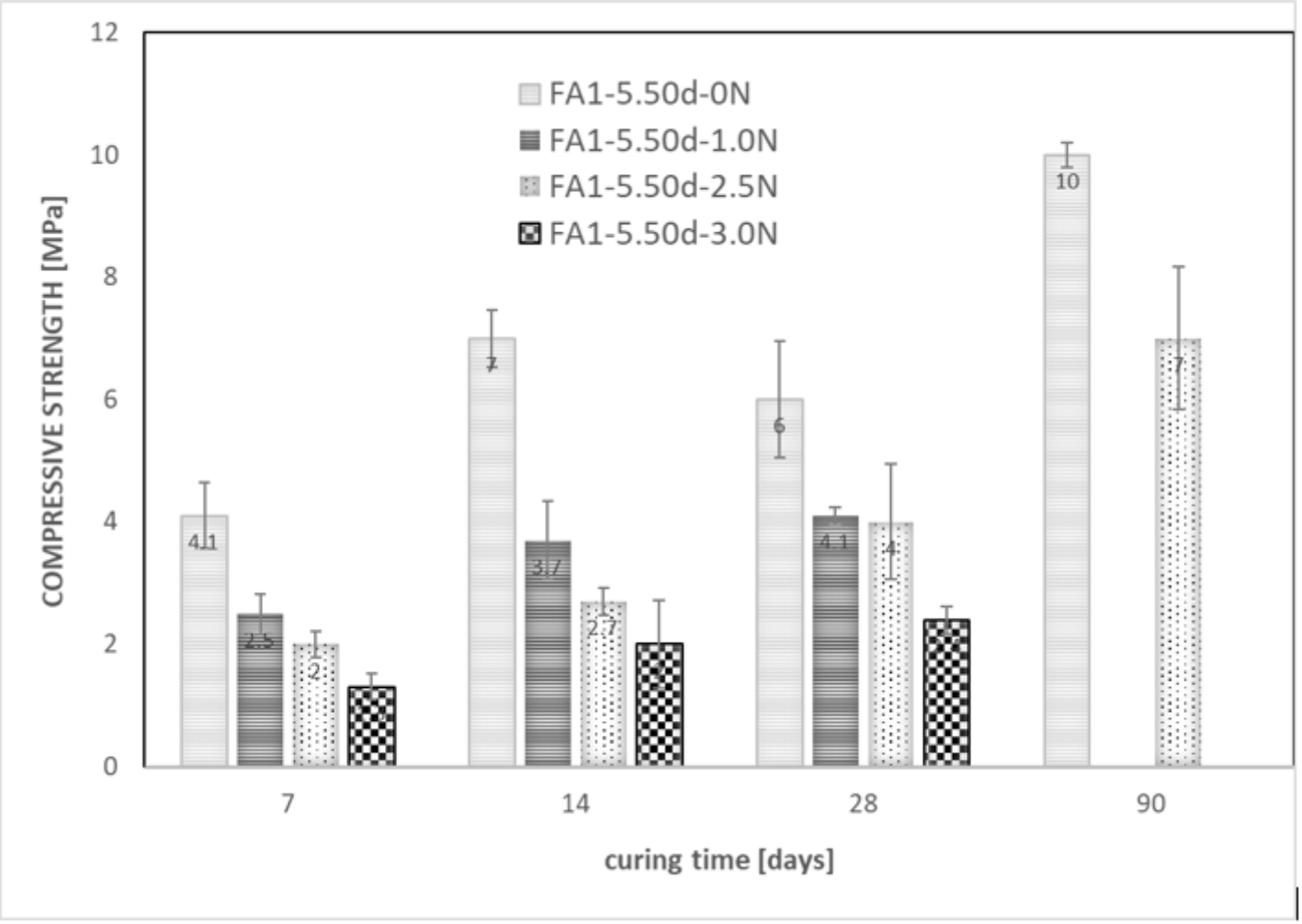


**Figure 15**

Compressive strength development in FA1-based geopolymers during the curing at d=5.50 (W:FA=0.57), different nitrate concentration

# Supplementary Files

This is a list of supplementary files associated with this preprint. Click to download.

- Onlinefloatimage1.png